Journal of Cell Science 113, 2187-2205 (2000)
Printed in Great Britain © The Company of Biologists Limited 2000
JCS1209

Arrested maturing multivesicular endosomes observed in a Chinese hamster ovary cell mutant, LEX2, isolated by repeated flow-cytometric cell sorting

Masato Ohashi[1,*], Ishido Miwako[1,2], Akitsugu Yamamoto[3] and Kuniaki Nagayama[1]

[1]Department of Molecular Physiology, National Institute for Physiological Sciences, Okazaki 444-8585, Japan
[2]Department of Biophysics, Faculty of Science, Kyoto University, Kyoto 606-8501, Japan
[3]Department of Physiology, Kansai Medical University, Osaka 570-8506, Japan
*Author for correspondence (e-mail: masato@nips.ac.jp)

Accepted 4 April; published on WWW 25 May 2000

SUMMARY

Chinese hamster ovary (CHO) cell mutants defective in the disintegration of endocytosed low-density lipoprotein (LDL) were isolated from mutagenized cells by repeated flow-cytometric cell sorting. After seven rounds of cell sorting, we obtained mutant pools, from which nine mutant clones were established. These mutant strains were all recessive, and were categorized into three complementation groups A, B, and C. The previously established CHO mutant, LEX1 (Lysosome-Endosome X1), fell into the complementation group A. One of the newly isolated mutants, LEX2, fell into the complementation group B, and showed slower degradation of RET-LDL than LEX1 cells. LEX2 showed prominence of well-elaborated multivesicular bodies (MVBs), positive for lysosomal glycoprotein-B/cathepsin D and cation-independent mannose 6-phosphate receptor (CI-MPR), yet negative for transferrin receptor or rab7. Endocytosed intact LDL accumulated in these CI-MPR-positive structures starting at 10-15 minutes of internalization and the accumulation reached completion at 20 minutes. Intermixing of separately internalized fluorescent LDLs between the LEX2 MVBs was slow and saturable at a lower level than observed between late endosomes/lysosomes in wild-type or in LEX1 cells. The receptor recycling pathway to the plasma membrane and the acidification of intracellular compartments were normal in LEX2 cells. These results are consistent with the idea that LEX2 cells are defective in the segregation and sequestration of contents at compartments equivalent to the transport intermediates, previously referred to as endosomal carrier vesicles or maturing MVBs. This MVB stage is likely to be an earlier stage than rab7-positive, lysosome-interacting late endosomes observed in LEX1 cells. Thus, LEX1 and LEX2 mutations could be considered as landmarks for these distinct late endocytic stages, and use of these cells in biochemical and molecular genetic analyses would help to understand the as yet unidentified details of late endocytic pathways including the MVB dynamics.

Key words: Endosome, Lysosome, Mutant, Multivesicular body, Mannose 6-phosphate receptor

INTRODUCTION

Various problems concerning the mechanisms and the regulation of the intracellular endocytic pathway in mammalian cells have yet to be solved (Gruenberg and Maxfield, 1995; Mellman, 1996; Mukherjee et al., 1997; Storrie and Desjardins, 1996). In particular, how the endocytic stages beyond early endosomes proceed has been a subject of considerable debate. Transport from early to late endosomes is mediated by relatively large, long-lived spherical vesicles showing an appearance of multivesicular bodies (MVBs). To emphasize their function as transport intermediates, these particular endosomal MVBs are referred to as endosomal carrier vesicles (ECVs; reviewed by Gu and Gruenberg, 1999; Kobayashi et al., 1998a). After formation on the early endosomal membrane, ECVs are carried along microtubules towards late endosomes. Since ECVs can fuse with late endosomes in cell-free content mixing assays, they are thought to fuse with preexisting cation-independent mannose 6-phoshpate receptor (CI-MPR)-positive late endosomes (Bomsel et al., 1990), which then interact with denser lysosomes (Bright et al., 1997). Alternatively, it is also suggested that endosomal MVBs mature and then fuse directly with the dense-core lysosomes in HEp-2 cells (Futter et al., 1996). Thus, although late endosomes are considered as a sorting station for the proteins destined for the *trans*-Golgi network (TGN) and the lysosomes (Gu and Gruenberg, 1999; Mellman, 1996; Mukherjee et al., 1997), precise functional differentiation and the structure-function relationships among MVBs, late endosomes and lysosomes have yet to be delineated. Perhaps determining the sorting efficiency and thus material distribution within these dynamic membrane compartments, proper interactions between these structures would be important for appropriate lysosomal digestive functions (Futter et al., 1996; Ohashi et al., 1999).

Although the identification of functional molecules

operating the late endocytic processes is obviously important to understand the mechanisms of the late endocytic traffic in mammalian cells, only a limited number of such molecules have been identified up to now: the *N*-ethylmaleimide-sensitive factor and perhaps an as-yet-undiscovered AAA-type ATPase are required for transport from early to late endosomes, as in many other intracellular fusion events (Mullock et al., 1998; Robinson et al., 1997). VAMP-7, a toxin-resistant SNARE, has recently been implicated in the pathway from early endosomes to late endosomes or from late endosomes to lysosomes (Advani et al., 1999). A small GTP-binding protein, rab7, functions either in the exit from early endosomes or in later stages of the endocytic pathway (Haas et al., 1995; Meresse et al., 1995; Ohashi et al., 1999; Press et al., 1998; Schimmoller and Riezman, 1993). Not only proteins, but also specific lipid species have increasingly been recognized as important factors in the late endocytic traffic (Bright et al., 1997; Kobayashi et al., 1988a, 1999; Odorizzi et al., 1998; Puri et al., 1999).

The combination of modern cell technologies such as mutant isolation techniques and the molecular genetic analysis of the isolated mutants has proven to be a powerful strategy to investigate the mechanisms of membrane traffic (Pryer et al., 1992; Schekman, 1992). This approach has been especially successful in studies using yeast genetics, where a number of functional molecules have been identified. Despite more difficulties in mammalian somatic cell genetics, the occasional lack of apparent homology in primary structures between yeast and mammalian proteins with a similar physiological function, and the possible differentiation of biochemistry in closely related biological processes between mammalian and yeast cells (Ohashi et al., 1995; Phillips et al., 1999) underscore the importance of functional screening of mammalian molecules in their own cellular environments. In particular, such a strategy in mammalian cells may identify not only those molecules responsible for basic functions commonly found in mammals and yeast, but also specialized molecules responding intercellular signaling within multicellular organisms. Furthermore, the importance of the endocytic pathway in human health merits the careful characterization and identification of functional molecules in mammalian cells.

We have previously isolated a CHO cell mutant, LEX1 (Lysosome-Endosome X1), showing a defect at one of the last membrane interaction steps from late endosomes to lysosomes (Ohashi et al., 1999). LEX1 cells were isolated primarily based on drug sensitivity by three-step screening in which analytical flow cytometry that detects the lysosomal degradation of a fluorescent low-density lipoprotein (LDL) within individual cells was used as the last screening step (Ohashi et al., 1999). In the present study, we employed a more direct application of the flow cytometric method, i.e. mutant screening by repeated flow-cytometric cell sorting. Using this method, we successfully isolated CHO cell mutants defective in the degradation of endocytosed LDL. The newly isolated mutants were categorized into three complementation groups A, B, and C. The previously isolated LEX1 mutant was found to fall into group A. We analyzed one of the newly established group B mutants, LEX2, in detail. LEX2 cells showed prominence of well-elaborated MVBs with the characteristics of an arrested form of ECV/maturing MVBs, and thus were suggested to have a defect at the ECV/MVBs. Discrete phenotypic differences between LEX1 and LEX2 cells have implied the existence of two separable stages in the late endocytic pathway: (1) sorting of proteins within the ECV/MVBs possibly coupled with consumption of the ECV/MVBs, and (2) direct interaction between rab7-positive late endosomes and the lysosomes. LEX1 and LEX2 mutations could be considered as landmarks for these late endocytic stages, and use of these cells in biochemistry and molecular genetic analysis would help to understand the as yet unidentified details of late endocytic pathways.

MATERIALS AND METHODS

Materials

RET-LDL was prepared as described previously (Ohashi et al., 1992), except that 22-(*N*-(7-nitrobenz-2-oxa-1,3-diazol-4-yl)amino)23,24-bisnor-5-cholen-3β-yl linoleate was substituted by 22-(*N*-(7-nitrobenz-2-oxa-1,3,-diazol-4-yl)amino)-23,24-bisnor-5-cholen-3β-yl *cis*-9-octadecenoate. LDL single-labeled with 22-(N-(7-nitrobenz-2-oxa-1,3,-diazol-4-yl)amino)-23,24-bisnor-5-cholen-3β-yl *cis*-9-octadecenoate (NBD-LDL) was prepared in the same procedure omitting octadecyl rhodamine B. DiO-LDL and R18-LDL were prepared as described previously (Ohashi et al., 1999). Rabbit polyclonal anti-CI-MPR antibody (Ueno et al., 1999) was kindly provided by Dr Takashi Ueno (Juntendo University). Monoclonal anti-syntaxin 6 antibody was purchased from Transduction Laboratories. Mouse monoclonal antibody (clone 12CA5) to a peptide epitope derived from the hemagglutinin (HA) protein of human influenza virus was from Roche Molecular Biochemicals. The other antibodies used were as described previously (Ohashi et al., 1999).

Isolation of mutant cells defective in the degradation of endocytosed LDL by repeated flow-cytometric cell sorting

Mutagenesis

Cell culture was done as described previously (Ohashi et al., 1992). CHO-K1 cells (subcloned) were plated (4×10^5/150 cm^2 bottle), cultured for two days, and were then mutagenized with 400-μg/ml ethyl methanesulfonate in culture medium for 16 hours at 37°C. After washing three times with culture medium, the cells were further cultivated in culture medium for one day. They were then replated into a 140-mm dish containing F12 medium supplemented with 5% lipoprotein deficient serum (Ohashi et al., 1992), 100-U/ml penicillin, and 10-μg/ml streptomycin, and were cultured for one day before the first flow-cytometric screening for mutants.

Repeated flow-cytometric cell sorting

For screening with a fluorescence-activated cell sorter (FACS), the mutagenized cells were made to endocytose a fluorescent LDL in a pulse (10 minutes), then chase incubations (20 minutes for RET-LDL, and 100 minutes for NBD-LDL) were performed, and the cells removed from dishes, as described previously (Ohashi et al., 1992), except that trypsinization was stopped with, and cells were washed and resuspended in 5% FCS, 20-mM NH_4Cl in Hanks' balanced salt solution in order to keep cell viability high enough during FACS sorting. Cells were sorted with a FACS Vantage system (Becton Dickinson, San Jose, CA/USA) according to single fluorescence analysis (FL1 at 530 nm, excitation at 488 nm; when NBD-LDL was used) or dual-parameter analysis (FL1 at 530 nm, FL2 at 585 nm, excitation at 488 nm; when RET-LDL was used). A linear sorting region (when NBD-LDL was used) or a rectangular sorting window whose sides were parallel to the axes of the histogram (when RET-LDL was used) was chosen to fulfill requirements derived from the theoretical consideration assuming that the probability of the number of recovered cells distributes binomially. The details of the theoretical consideration are described in the Appendix to this paper. Each round of sorting process was monitored and evaluated by calculating the net number of screened mutagenized cells and the maximum clonal

number of survived wild-type cells based on the same theoretical consideration. After sorting, the selected cells were collected in growth medium and were cultured. The FACS sorting procedure was repeated until cell populations showing the mutant phenotype were obtained.

Generation of cells expressing HA-tagged, wild-type or mutant rab7

The human rab7 ORF was PCR-amplified from a human cDNA library with the Expand High Fidelity PCR System (Roche) using primers, 5′-GGATGACCTCTAGGAAGAAA-3′ and 5′-CTCAGCA-ACTGCAGCTT-3′. The PCR products were TA-cloned into a T-vector generated from pBluescript SK– (Stratagene) using the *Eco*RV site (Marchuk et al., 1991). A resulting construct, pTA-rab7, was confirmed by DNA sequencing to harbour in the reverse direction a complete ORF encoding the wild-type human rab7 protein (Vitelli et al., 1996). An HA-tag was introduced to the N terminus of the rab7 within pTA-rab7 by a PCR-based method (Imai et al., 1991) using primers, 5′-GTCCCAGACTACGCTATGACCTCTAGGAAGAAAG-TG-3′ and 5′-GTCGTATGGGTACATCCAATCGAATTCCTGC-3′, producing pTA-NHArab7. Then, a constitutively active mutation Q67L (numbering according to the original rab7 sequence; Vitelli et al., 1997) was introduced into the rab7 within pTA-NHArab7 by PCR-based site-directed mutagenesis (Imai et al., 1991), using primers, 5′-TGGAACGGTTCCAGTCT-3′ and 5′-GTCCTGCTGTGTCCCATA-3′, generating pTA-NHArab7Q67L. These sequence modifications and other sequence integrities were confirmed by DNA sequencing. From these constructs, the HA-tagged rab7 (NHArab7) and the HA-tagged rab7Q67L (NHArab7Q67L) sequences were subcloned into a mammalian expression vector pCI-neo (Promega) using the *Eco*RI-*Sal*I sites, producing pCI-neo-NHArab7 and pCI-neo-NHArab7Q67L, respectively. The NHArab7 and NHArab7Q67L fragments were also subcloned into a retroviral vector pBabe-puro (Morgenstern and Land, 1990) using the *Bam*HI-*Sal*I sites, producing pBabe-puro-NHArab7 and pBabe-puro-NHArab7Q67L, respectively.

Cells were transfected with pCI-neo-NHArab7 or pCI-neo-NHArab7Q67L using LipofectAMINE (Life Technologies) according to the manufacturer's instructions. Alternatively, the NHArab7 and the NHArab7Q67L sequences with the puro marker sequence were packaged into ecotropic viruses from the pBabe-puro constructs, and were introduced by retrovirus-mediated gene transfer (Kitamura et al., 1995) into CHO wild-type and mutant cells that are expressing mouse ecotropic retroviral receptor (Miwako and Ohashi, manuscript in preparation). Pools of cells stably expressing NHArab7 or NHArab7Q67L were obtained by selecting the transfected cells in medium containing 500-μg/ml G418 (Life Technologies) for the neo marker, or in medium containing 12-μg/ml puromycin•2HCl (Sigma) for the puro marker. The expression of HA-tagged rab7 proteins of expected molecular size was confirmed by western blotting of cell extracts using the anti-HA epitope and anti-rab7 antibodies (data not shown).

Immunofluorescence

Before all analyses, including immunofluorescence, cells were pretreated for one day with medium containing 5% lipoprotein deficient serum (Ohashi et al., 1992). Cell fixation and immunofluorescence staining were done as described previously (Ohashi et al., 1999). For NHArab7Q67L staining using anti-HA antibody, cells were not pretreated with digitonin before fixation. Fluorescence laser-scanning confocal microscopy was done as described previously (Ohashi et al., 1999); images were taken with an optical section set at <0.8 μm unless otherwise mentioned. Semiquantification of colocalization in double fluorescence microscopy based on a fluorescence intensity analysis was performed essentially as described previously (Ohashi et al., 1999). In the case of samples double-labeled with R18- and DiO-LDL, each image data was compensated for leakage of emission light from one fluorophore into the other's detector. The fraction of leakage was measured with the image data of the cells labeled with one fluorophore only, then was subtracted from the images of dual-labeled samples with a Carl Zeiss LSM510 program. In our experiments, 20% of the R18 fluorescence was detected in the green image data, and 18% of the DiO fluorescence was detected in the red image data.

Electron microscopy

Conventional and immuno-electron microscopy was done as described previously (Ohashi et al., 1999) except that permeabilization of cells in 0.25% saponin for immuno-electron microscopy was replaced by a freezing and thawing method in liquid nitrogen after cryo-protection in 0.1 M Na-phosphate buffer (pH 7.4, PB) containing 35% sucrose and 14% glycerol (Mrini et al., 1995). For double immunostaining experiments, cells were treated with the blocking solution containing corresponding primary antibodies overnight. After washing in PB containing 0.005% saponin, the cells were incubated with goat anti-rabbit IgG labeled with colloidal gold (1.4 nm diameter) and biotinylated anti-mouse IgG in the blocking solution for 2 hours. After washing in PB containing 0.005% saponin, the cells were treated with streptavidin conjugated with horseradish peroxidase (HRP) for 30 minutes. The cells were washed with PB for 10 minutes six times, and fixed with 1% glutaraldehyde in PB for 10 minutes. The gold labeling was intensified using a silver enhancement kit (HQ silver, Nanoprobes) for 7.5 minutes at 20°C in the dark. After washing, HRP labeling was visualized by DAB reaction. The cells were post-fixed in 0.5% OsO_4 for 90 minutes, stained with 2% uranyl acetate in 70% ethanol for 2 hours, and were embedded in epoxy resin. Ultra-thin sections were stained with uranyl acetate.

Acridine Orange staining

Cells were washed four times with Hanks' solution at 37°C and were treated with 0.5-μg/ml acridine orange in Hanks' solution for 20 minutes at 37°C. The cells were washed five times with ice-cold PBS, mounted in PBS, and were observed under an Olympus IX70 microscope equipped with an LCPlanFl60× objective and a rhodamine filter set (Olympus, Tokyo/Japan).

Other methods

The quantitation of the cellular uptake and degradation of RET-LDL based on analytical flow cytometry was done as described previously (Ohashi et al., 1992), except that an EPICS XL cytometer (Beckman Coulter, Inc., Fullerton/USA; excitation at 488 nm, FL1=525 nm, FL2=575 nm) was used and calculations described therein were done with measurement at these emission wavelengths accordingly. Lysosomal enzyme activities were determined according to the method of Merion and Sly (1983).

RESULTS

Isolation of CHO cell mutants defective in the lysosomal degradation of LDL by repeated flow-cytometric cell sorting

For repeated flow-cytometric mutant screening, we used two types of fluorescent LDLs to isolate CHO cells defective in post-uptake LDL degradation. One is RET-LDL, which was previously designed to detect lysosomal disintegration of LDL by flow cytometry (Ohashi et al., 1992). Although the probe had been well characterized, preliminary experiments indicated that the resolution of cells with different characteristics in RET-LDL degradation was not good enough. To overcome this problem, we used a second fluorescent LDL, NBD-LDL. In contrast with RET-LDL flow cytometry detecting the lysosomal degradation of RET-LDL, NBD-LDL flow cytometry detects the release of NBD from cells: After

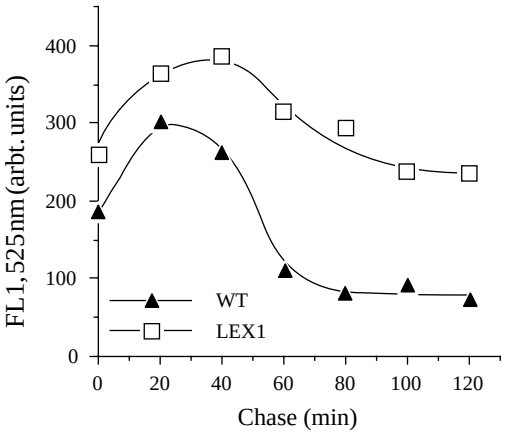

Fig. 1. Flow-cytometric analysis of wild-type and LEX1 cells that endocytosed NBD-LDL in a pulse-chase experiment. Wild-type (WT) and LEX1 cells (LEX1) endocytosed NBD-LDL (10 μg/ml) in a 10-minute pulse. Then chase incubations were performed for various times. After chase, the cells were removed from the dishes and were subjected to analytical flow cytometry for NBD fluorescence. Note that the initial rise in fluorescence during the chase period possibly resulted from both internalization of cell-surface-bound NBD-LDL and the relief of NBD-LDL self-quenching upon degradation. At each data point, 3,000 cells were analyzed. The mean fluorescence is shown.

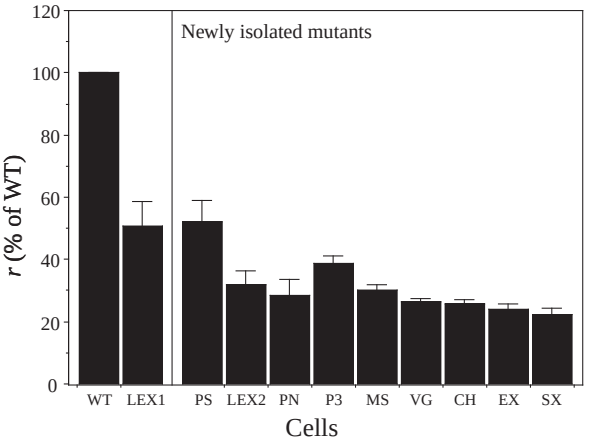

Fig. 2. Disintegration of RET-LDL was impaired in the newly isolated mutants. Wild-type (WT), LEX1, and indicated newly isolated mutant cells were made to endocytose RET-LDL in a 10-minute pulse, followed by a 20-minute chase. The cells were analyzed for RET-LDL degradation by analytical flow cytometry. For each determination, 3,000 cells were analyzed. Value *r*, indicating the extent of disintegration of RET-LDL in cells was calculated from dual-parameter histograms, and then is expressed as a percentage of the value of wild-type cells. The mean of three experiments is shown. Bars indicate s.e.m.

degradation of NBD-LDL by lysosomal hydrolases, a substantial part of NBD-cholesterol liberated from NBD-LDL appears to be transported to the cell surface and then released from the cells after a sufficiently long chase time (Ohashi et al., 1992). Thus fluorescence from cells that have endocytosed NBD-LDL decreases as chase time goes (Ohashi et al., 1992). As was expected, apparently due to defective lysosomal LDL degradation, this decrease was slower in the previously isolated mutant, LEX1, than in wild-type cells (Fig. 1).

Although the NBD-LDL analysis gives more ambiguous results as to lysosomal LDL degradation than the RET-LDL analysis, NBD-LDL was used so as to keep the net size of screened cells large for initial three rounds of screening before more specific RET-LDL was employed at later rounds (see the Appendix). In order to assess the feasibility of mutant isolation by repeated flow-cytometric cell sorting using these probes, we first simulated the mutant isolation process by calculation, assuming that the probability of the number of recovered cells after sorting distributes binomially (see Appendix). LEX1 cells were used as a reference, and simulation was done for mutant cells showing a LEX1-like phenotype. As a result, it was estimated that, after seven to eight rounds of flow-cytometric cell sorting, a mutant pool would be obtained from original mutagenized cells containing expected LEX1-like mutant cells at a frequency of 10^{-6}~10^{-5}.

Screening for CHO cells defective in the post-uptake degradation of LDL was done under conditions essentially in accordance with the simulation, and was monitored by calculating the mutant selectivity and the net number of screened mutagenized cells at each round of sorting (see Appendix). The selection was started with mutagenized cells in six culture bottles. Cells from each starting bottle were handled independently (thus in six sets) throughout the sorting process in order to prevent only a subset of mutants or unrelated cells from dominating the whole population of the selected cell pools. After three rounds of sorting with NBD-LDL and subsequent four rounds with RET-LDL, monitoring results predicted that sorting had been sufficiently repeated. Indeed, at this point, all cell populations from the six sets showed slowed RET-LDL disintegration (data not shown). With each set of mutagenesis, 2.5×10^5 cells (net) were estimated to have been screened. Thus, about 1.5×10^6 cells were screened in total. Randomly taking a few clones per set by limiting dilution, a total of 13 clones were isolated, among which nine clones (PS, LEX2, PN, P3, MS, VG, CH, EX, SX) exhibited RET-LDL disintegration as slow as, or slower than LEX1 cells (Fig. 2).

Complementation analysis of mutants identified three complementation groups

The phenotypes of the newly isolated mutants were partially characterized for preliminary categorization (summarized in Table 1). There was no recognizable difference in the distribution of an early endosome marker, transferrin receptor (Yamashiro et al., 1984), in any of the newly established mutants (data not shown). PS cells exhibited LEX1-type redistribution of late endosome/lysosome marker proteins: Like in LEX1 cells (Ohashi et al., 1999), a late endosome/lysosome marker, lgp-B, and a lysosome enzyme, cathepsin D, were observed colocalized in a perinuclearly concentrated aggregative staining (data not shown). A late endosome marker, rab7, was also observed in a perinuclearly concentrated aggregate in PS cells (data not shown). LEX2 and PN cells showed an alteration of lgp-B distribution but not of rab7 (data not shown, see later sections for detailed analysis of LEX2). The remaining newly isolated mutant cells were stained more or less in the wild-type pattern for these late endosome/lysosome marker proteins (data not shown).

Table 1. Summary of complementation and partial phenotypic analyses of the mutant cells used in this study

Cell		lgp-B/ cathepsin D distribution	rab7 distribution	Acridine Orange staining	Transferrin receptor distribution	Electron microscopy	Defective lysosomal enzymes*
Complementation group	Strain						
WT	Wild type	Particles (scattered)	Particles (scattered)	Particles (scattered)	Loose perinuclear concentration	Normal	–
A	LEX1‡	Agg.	Agg.	Agg.	w.t.	Agg.	Glu, Gal
	PS	Agg.	Agg.	Agg.	w.t.	Agg.	–
B	LEX2	Loosely gathered dots	w.t.	Loosely gathered dots	w.t.	MVB	–
	PN						–
	MS	w.t.	w.t.	w.t.	w.t.	MVB and/or vac.	–
	CH						–
	VG						–
	EX	w.t.	w.t.	w.t.	w.t.	w.t.	–
	SX						–
C	P3	w.t.	w.t.	w.t.	w.t.	Vac.	Hex, Glu, Gal

Wild-type, LEX1, and newly isolated mutant cells were characterized by immunofluorescence staining, Acridine Orange staining, electron microscopy, and lysosomal enzyme activity determination. The newly isolated mutants are categorized into complementation groups A, B, and C based on complementation analysis for RET-LDL disintegration. w.t., wild-type-like; Agg., a perinuclear vesicle aggregate like in LEX1 cells; MVB, well-developed multi-vesicular bodies; Vac., prominent vacuoles. *Hex, β-hexosaminidase; Glu, β-glucuronidase; Gal, β-galactosidase. ‡Partially from a previous report (Ohashi et al., 1999).

By electron microscopy, LEX2, PN, MS, CH, VG and P3 cells were characterized by the prominence of MVBs and/or vacuoles. In LEX2, PN, MS, and CH cells, a number of highly developed MVBs were observed (Fig. 3A, and data not shown). On the other hand, in VG and P3 cells, vacuoles scattered within the cytoplasm were frequently seen (Fig. 3B, and data not shown). MVBs were also prominent in VG cells, although less in frequency and less well-elaborated in multivesicular morphology than were observed in LEX2, PN, MS, or CH cells (data not shown). Other membraneous organelles, such as the Golgi and mitochondria appeared normal in these cells (Fig. 3B, and data not shown). EX and

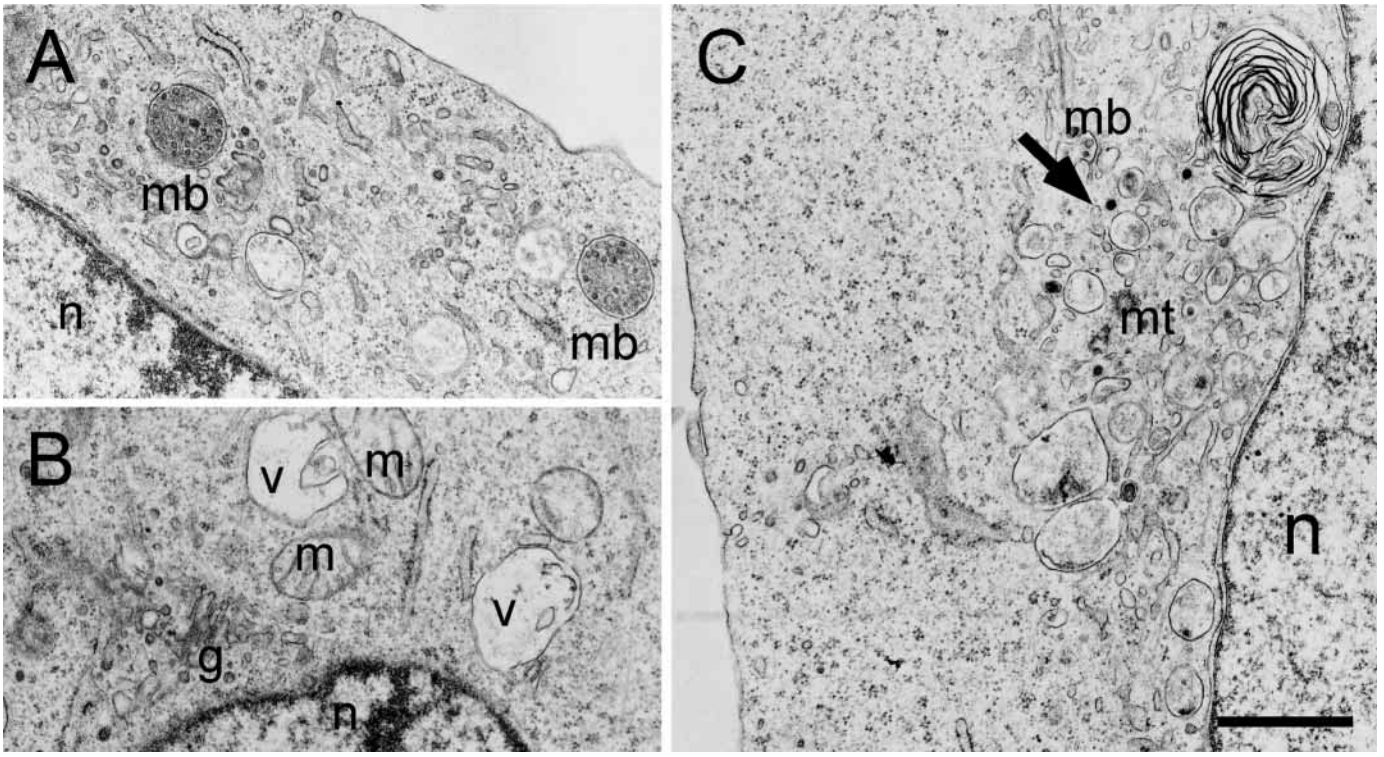

Fig. 3. Conventional electron microscopy revealed existence of various abnormal vesicles in LEX2 and other newly isolated mutants. Conventional electron micrographs of a LEX2 cell (A), a VG cell (B), and a PS cell (C). The arrow in C indicates a heterogeneous vesicle aggregate formed around the MTOC. mb: multivesicular body, mt: MTOC, n: nucleus, v: vacuole, m: mitochondrion, g: Golgi apparatus. Bar, 1 μm.

Table 2. Lysosomal enzyme activity of the mutant cells

CHO Strain	Relative lysosomal enzyme activity			
	Hex	Glu	Pho	Gal
Wild type	1	1	1	1
LEX1	0.84	0.36	1.02	0.39
PS	1.1	0.78	1.03	1.22
LEX2	0.93	0.81	0.93	0.96
PN	0.96	0.85	1.11	1.11
MS	0.91	0.87	1.03	0.78
CH	0.79	0.79	0.97	0.91
VG	0.73	0.75	1.14	0.81
EX	0.92	0.83	1.28	0.81
SX	1.04	0.94	1.32	0.86
P3	0.28	0.61	1.19	0.28

Relative lysosomal enzyme activities are expressed relative to the wild-type activity (=1). The mean of values from three samples is shown. The values showing a significant difference from the wild-type value are double underlined ($P<0.05$ by *t*-test). Hex, β-hexosaminidase; Glu, β-glucuronidase; Pho, acid phosphatase; Gal, β-galactosidase.

SX cells showed more or less wild-type morphology by conventional electron microscopy.

In accordance with the fluorescence microscopic observations, PS cells showed a perinuclear aggregate of heterogeneous vesicles formed around the microtubule organization center (MTOC; Fig. 3C, mt), much like that in LEX1 cells (Ohashi et al., 1999). Other membraneous organelles appeared normal in PS cells (Fig. 3C, and data not shown).

Acridine Orange stained the mutant cells in the same pattern as in the lgp-B stain, suggesting no gross perturbation of the acidification of endocytic compartments stained with lgp-B in these mutants.

P3 cells showed significantly reduced activities of three lysosomal enzymes (β-hexosaminidase, β-galactosidase, and β-glucuronidase) out of four tested (Table 2). However, all of the other newly isolated mutants exhibited normal specific lysosomal enzyme activities (Table 2).

Considering these phenotypic similarities among the newly isolated mutants and LEX1 cells, the mutants were tested for mutual complementation of RET-LDL degradation by somatic cell hybridization (Table 1). They were first tested for dominance over wild-type cells. The mutants and wild-type cells transfected with a dominant selectable marker, bsr, hph, or neo, were fused and mutant-wild type hybrids selected and analyzed by flow cytometry for RET-LDL disintegration as previously described (Ohashi et al., 1999). All mutant-wild type hybrids showed disintegration of RET-LDL almost as efficient as wild type-wild type homotypically fused cells, showing that all of the newly isolated mutants are recessive to wild-type cells (Tables 3 and 5, and data not shown).

Since newly isolated PS cells showed a perinuclear lgp-B-positive aggregate similar to that observed in LEX1 cells, PS and LEX1 cells were first fused and the resultant hybrids tested for complementation by flow cytometry for RET-LDL disintegration. PS-LEX1 hybrids showed defective RET-LDL disintegration similar to that shown by PS-PS or LEX1-LEX1 homotypically fused cells, much less efficient than that shown by LEX1- or PS-wild type hybrids (Table 3). Thus, the defective RET-LDL disintegration seen in PS cells was not complemented by fusion with LEX1 cells. The result clearly showed that PS cells fall into the same complementation group (group A) as LEX1 cells.

Mutants with other phenotypic characteristics were analyzed in the same manner. LEX2 and PN mutants, characterized by highly elaborated MVBs, were hybridized. LEX2-PN hybrids showed the defective RET-LDL disintegration (data not shown), showing that they are in the same complementation group.

So far examined, EX and SX cells showed wild-type-like phenotypes in all analyses except for RET-LDL disintegration. Hybrids between EX and SX cells exhibited the defective disintegration of RET-LDL (data not shown), showing that they are in the same complementation group. Furthermore, EX, MS, CH, and VG cells were fused in all possible pairings and it was shown that the defective RET-LDL disintegration was not complemented in any pairs (data not shown). Thus, all of these five mutants (EX, SX, MS, CH, and VG) belong to one complementation group.

Next, LEX2 and EX (representing the five mutants just above) cells were tested for complementation. Despite the apparent difference between the phenotypes these mutants had exhibited, the hybrid formation did not complement the defective disintegration of RET-LDL (Table 4). Thus, all of LEX2, PN, MS, CH, VG, EX, and SX cells fall into the same complementation group designated here as group B. It is noteworthy that the mutants of complementation group B exhibited vacuole/MVBs showing various degrees of elaboration with a rather continuous spectrum (see above), despite their being of one complementation group.

Finally, PS (group A), LEX2 (group B), and P3 (characterized by partially reduced lysosomal enzyme activities) cells were mutually fused and tested for complementation. All hybrids showed the complementation of RET-LDL disintegration (Table 5), demonstrating that these mutant cells fall into three different complementation groups (A, B, and C).

Table 3. Complementation analysis between LEX1 and PS cells

Mutant with bsr marker	Mutant with hph marker		
	WThph	LEX1hph	PShph
WTbsr	100	86	98
LEX1bsr	86	54	60
PSbsr	81	56	52

Hybrid cells were made by fusion of indicated pairs of cells with the indicated dominant selectable markers. They were analyzed by flow cytometry for RET-LDL disintegration. WT, wild type. The r values are shown in percentages of that of homotypically fused wild-type cells. Underlined, complemented.

Table 4. Complementation analysis between LEX2 and EX cells

Mutant with bsr marker	Mutant with hph marker		
	WThph	LEX2hph	EXhph
WTbsr	100	N.D.*	N.D.*
LEX2bsr	N.D.*	35	34
EXbsr	N.D.*	36	30

See footnote to Table 3. The r values are shown in percentages of that of homotypically fused wild-type cells. Underlined, complemented. N.D., not done in this particular experiment. *Data not shown.

Table 5. Complementation analysis between PS, LEX2 and P3 cells

	Mutant with hph marker			
Mutant with bsr marker	WThph	PShph	LEX2hph	P3hph
WTbsr	100	94	93	101
PSbsr	88	56	85	92
LEX2bsr	86	81	28	85
P3bsr	84	95	88	53

See footnote to Table 3. The r values are shown in percentages of that of homotypically fused wild-type cells. Underlined, complemented.

LEX2 cells showed slower degradation of RET-LDL than LEX1 cells

For most extensive analysis, we had chosen one newly established mutant, LEX2, because this mutant fell into a different complementation group from that of LEX1 cells, and was among those exhibiting most remarkably different phenotypes from LEX1 cells (Table 1).

As the first step of characterization, the uptake and the degradation of RET-LDL by cells were examined. As shown previously (Ohashi et al., 1999), LEX1 cells exhibited an about 50% higher uptake of RET-LDL than wild-type cells during a 10-minute pulse (Fig. 4A), and the degradation of RET-LDL in LEX1 cells was slower than in wild-type cells (Fig. 4B,C). In LEX2 cells, The uptake of RET-LDL during a 10-minute pulse was comparable to that by wild-type cells (Fig. 4A, ~80% of the wild-type value); however, RET-LDL degradation was even slower than in LEX1 cells (Fig. 4B,C).

CI-MPR, lysosomal glycoprotein-B (lgp-B) and cathepsin D, but not rab7 were colocalized in larger vesicles in LEX2 cells

The morphology of endocytic compartments of LEX2 cells was analyzed by fluorescence microscopy. As mentioned earlier, there was no recognizable difference in the distribution of an early endosome marker, transferrin receptor, in LEX2 cells (data not shown). However, in LEX2 cells, a late endosome/lysosome marker, lgp-B, and a lysosome enzyme, cathepsin D, were observed colocalized in scattered dots, larger in appearance than in wild-type cells, and loosely gathered together near the nucleus in the cytoplasm (Fig. 5D,F, and data not shown). In control wild-type cells, they were observed colocalized in small dots all over the cytoplasm (Fig. 5B, and Ohashi et al., 1999).

Furthermore, CI-MPR, a marker protein for late endosomes and other compartments involved in transport between the TGN and endosomes (Brown and Farquhar, 1987; Griffiths et al., 1988), showed a prominent redistribution in LEX2 cells. In wild-type cells, CI-MPR showed a perinuclear Golgi-type distribution (Fig. 5A) closely associated with the distribution of syntaxin 6 (data not shown), known to be present primarily in the TGN (Bock et al., 1997). Only a minor population of CI-MPR was colocalized with lgp-B in wild-type cells (Fig. 5A,B). By marked contrast, in LEX2 cells, CI-MPR was almost totally redistributed from the Golgi pattern into larger scattered dots (Fig. 5C), which were colocalized with lgp-B in the altered distribution (Fig. 5C,D). Some lgp-B-positive dots appeared negative for CI-MPR (Fig. 5C,D) About 10 to 20 dots double-positive for CI-MPR and lgp-B of various size in each LEX2 cell were identified by 3-D-scanning confocal microscopy (Fig. 5E,F). Despite this remarkable redistribution of CI-MPR, LEX2 cells contained a comparable amount of CI-MPR to that in wild-type cells (about 80% of the wild type, normalized by total protein) as shown by quantitative western blotting analysis (data not shown). The redistribution of CI-MPR into the lgp-B-positive dots was specific to LEX2 cells, and was statistically significant as shown by semiquantitative colocalization analysis

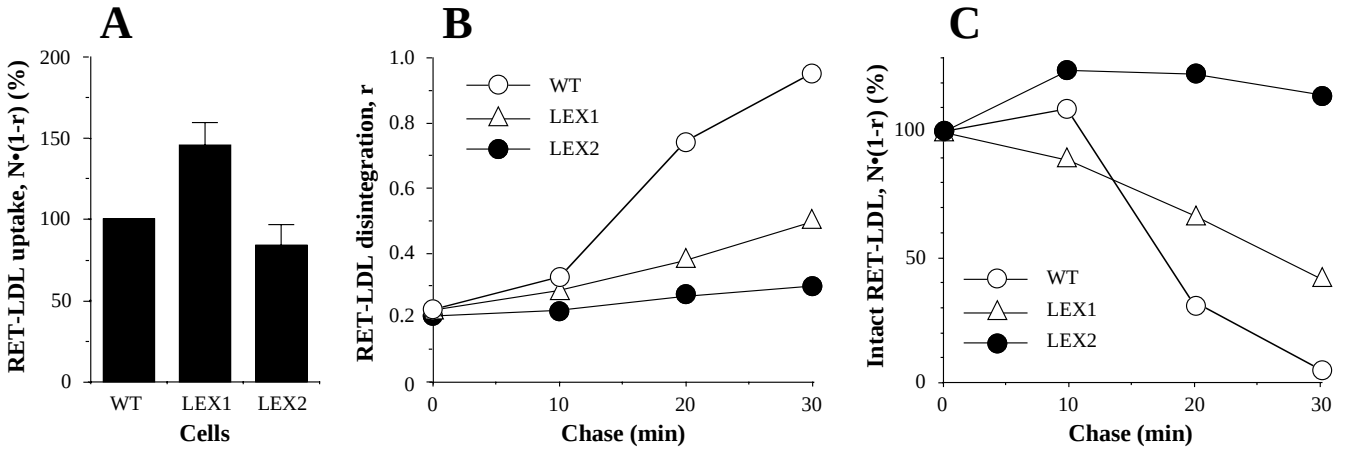

Fig. 4. LEX2 cells showed slower degradation of RET-LDL than LEX1 cells. (A) RET-LDL uptake during a 10-minute pulse. Wild-type (WT), LEX1 and LEX2 cells endocytosed RET-LDL (10 μg/ml) for 10 minutes at 37°C. The cells were then subjected to dual-parameter flow cytometry. Three thousand cells were analyzed for each determination. The value N•(1-r), indicating the mean amount of intact RET-LDL within a cell, was calculated from dual-parameter histograms. The values of LEX1 and LEX2 cells are expressed as percentages of that of wild-type cells. The mean ± s.e.m. (*n*=5(LEX1), 4(LEX2)) is shown. (B,C) Time course of RET-LDL disintegration. Wild-type (WT), LEX1 and LEX2 cells endocytosed RET-LDL (10 μg/ml) for 10 minutes at 37°C. Then chase incubations were performed at 37°C for various times as indicated. The cells were then subjected to dual-parameter flow cytometry. Three thousand cells were analyzed for each determination. Values *r*, indicating the extent of disintegration of RET-LDL within a cell (B), and N•(1-r), indicating the mean amount of intact RET-LDL within a cell (C), were calculated from dual-parameter histograms. In C, values are expressed as percentages of the value at time zero of chase. The mean of three experiments is shown.

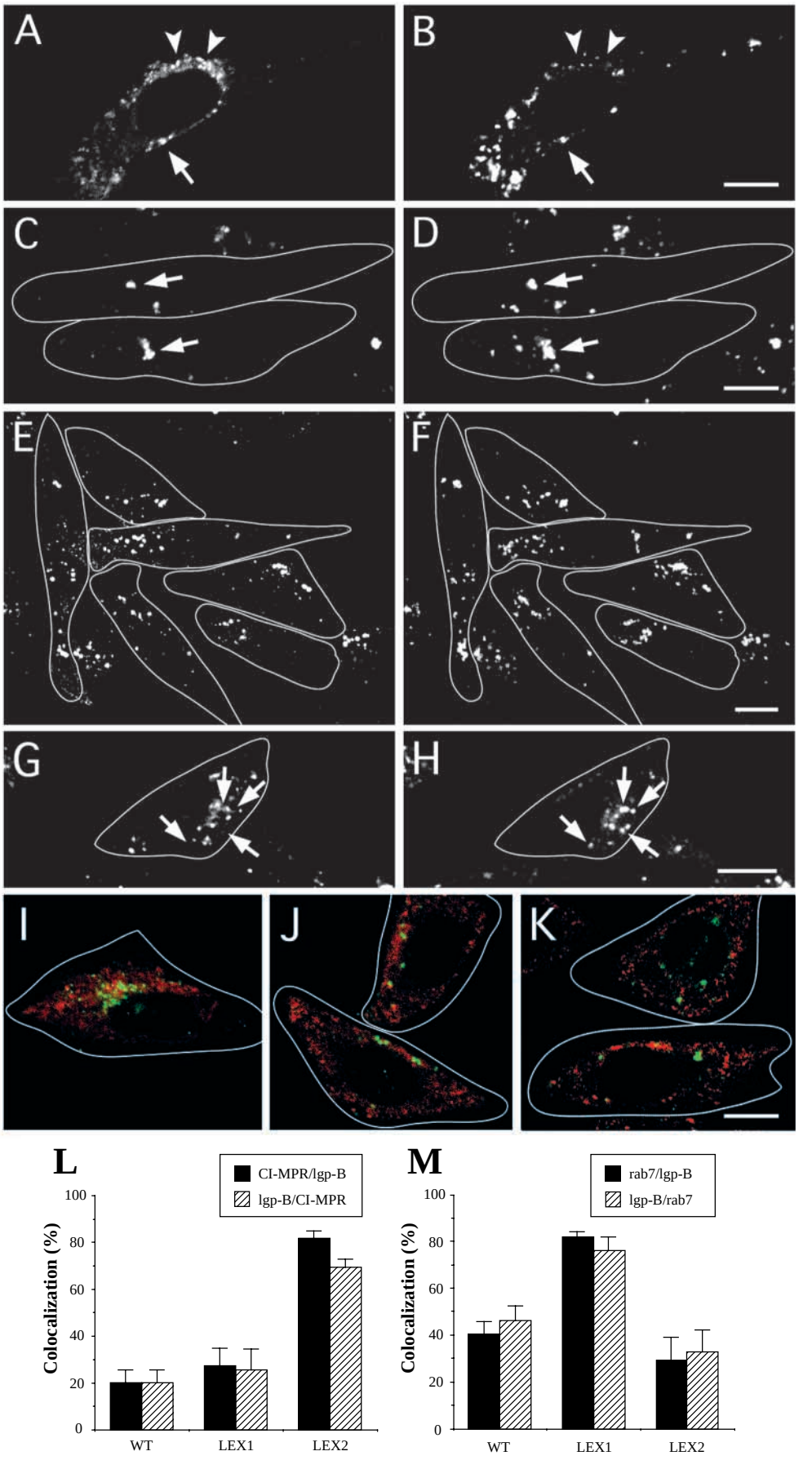

Fig. 5. CI-MPR, lgp-B and cathepsin D, but not rab7 were colocalized in larger vesicles in LEX2 cells. (A-F) CI-MPR (A,C,E) and lgp-B (B,D,F) were immunofluorescently double localized in wild-type cells (A,B) and in LEX2 cells (C,D and E,F). Arrowheads in A and B indicate CI-MPR-positive, lgp-B-negative compartments. Arrows indicate the colocalization of CI-MPR and lgp-B. In E and F, whole-cell projected figures, reconstituted from 3-D confocal scanning images (optical slice <0.7 μm, interval=0.7 μm), are shown. Bars, 10 μm. (G,H) Rab7 (G) and lgp-B (H) were immunofluorescently double localized in LEX2 cells. Arrows indicate lgp-B-positive, rab7-negative compartments. Bar, 10 μm. (I,J) NHArab7 (red) and CI-MPR (green) were immunofluorescently double localized using anti-HA-tag mouse monoclonal and anti-CI-MPR rabbit polyclonal antibodies in wild-type (I) and LEX2 (J) cells both expressing NHArab7 from the pCI-neo construct. (K) NHArab7Q67L (red) and CI-MPR (green) were immunofluorescently double localized in LEX2 cells expressing NHArab7Q67L by retrovirus-mediated gene transfer. Bar, 10 μm. Some cell profiles are drawn. (L) The colocalization of CI-MPR and lgp-B was enhanced in LEX2 cells but not in LEX1 cells. CI-MPR and lgp-B were immunofluorescently double localized and the colocalization was expressed semiquantitatively as described in Materials and Methods. The mean of data from six (WT, LEX1) or five (LEX2) cells is shown. Bars indicate s.e.m. (M) The colocalization of rab7 and lgp-B was enhanced in LEX1 cells but not in LEX2 cells. Rab7 and lgp-B were immunofluorescently double localized and the colocalization was expressed semiquantitatively as described in Materials and Methods. The mean of data from five (WT, LEX1) or seven (LEX2) cells is shown. Bars indicate s.e.m.

(Fig. 5L): a more than threefold increase of colocalization of CI-MPR with lgp-B was observed in LEX2 cells; however, by the same analysis, such an elevated colocalization was not observed in LEX1 cells. In spite of the redistribution of CI-MPR, the TGN integrity appeared to be preserved in LEX2 cells; the distribution of neither syntaxin 6 nor BODIPY FL C5-ceramide (a marker for the TGN (Pagano et al., 1991)) was altered (data not shown). Thus the CI-MPR redistribution was selective for this molecule.

Interestingly, indirect immunofluorescence staining for a late endosome marker, rab7 (Chavrier et al., 1990), did not show any redistribution in LEX2 cells (Fig. 5G). The lgp-B-positive larger dots in LEX2 cells did not colocalize with rab7 (Fig. 5G,H). This has made a marked contrast with the case of LEX1 cells as shown by semiquantification of colocalization: while about twofold elevation of the colocalization of rab7 with lgp-B over wild-type cells was observed in LEX1 cells, no elevation was observed in LEX2 cells (Fig. 5M).

The localization between rab7 and CI-MPR was also compared. Since both of the antibodies we used to stain endogenous rab7 and CI-MPR were rabbit polyclonal, cells expressing human rab7 N-terminally tagged with the HA epitope (NHArab7), or its constitutively active derivative harbouring a Q67L mutation (Vitelli et al., 1997; NHArab7Q67L) were generated for double staining. These cells expressing exogenous rab7 were double stained for CI-MPR and the HA-tagged proteins using anti-CI-MPR rabbit polyclonal and anti-HA-tag mouse monoclonal antibodies. The active GTP-state rab7Q67L is expected to more preferentially associate with membranes onto which rab7 exerts its function. The HA-tagged rab7 proteins were distributed like endogenous rab7: in particular, the characteristic perinuclear aggregate in LEX1 cells was observed with these tagged proteins (M. Ohashi, unpublished observations). The distributions of NHArab7 and CI-MPR did not substantially overlap each other in wild-type cells (Fig. 5I). In LEX2 cells, the characteristic dotty distribution of CI-MPR was largely not affected by the expression of these proteins (Fig. 5J, and data not shown), and these CI-MPR-positive dots did not substantially overlap with the distribution of NHArab7 (Fig. 5J) or NHArab7Q67L (Fig. 5K).

Endocytosed intact LDL is accumulated in MVBs positive for CI-MPR and lgp-B in LEX2 cells

In order to examine if endocytosed intact LDL accumulates in the unusual CI-MPR-, lgp-B-positive dots in LEX2 cells, CI-MPR and endocytosed unlabelled LDL were double immunolocalized (Fig. 6). LDL immunolocalization should detect only undegraded LDL that retains its antigenicity. At 20 minutes of chase of cell-surface-bound unlabelled reconstituted LDL, undegraded LDL was still visible in both wild-type and LEX2 cells. While, in wild-type cells, a majority of LDL was not colocalized with CI-MPR at this time (Fig. 6A,B), most of immunoreactive LDL was observed in the CI-MPR-positive dots in LEX2 cells (Fig. 6C,D). The elevated colocalization of LDL and CI-MPR in LEX2 cells was also confirmed by statistic analysis on semiquantitative colocalization data (Fig. 6E).

The time course of endocytosed LDL delivery to the CI-MPR-positive dots was followed in experiments where LDL prebound to cell-surface receptors was endocytosed by LEX2 cells for various periods. Internalized LDL was recognized to accumulate in the CI-MPR-positive dots starting at about 10-15 minutes of uptake, and the accumulation in the dots rapidly reached completion at about 20 minutes in LEX2 cells (cf. Fig. 6C,D, and data not shown). The colocalization of endocytosed LDL and CI-MPR was still observed at an internalization time as long as 90 minutes (data not shown). Yet, these CI-MPR-positive dots are not likely to be dead-end structures, since, after a longer chase of about 2-3 hours, the fluorescence of endocytosed R18-LDL and CI-MPR started being observed in separate dots (data not shown). On the other hand, the colocalization of endocytosed

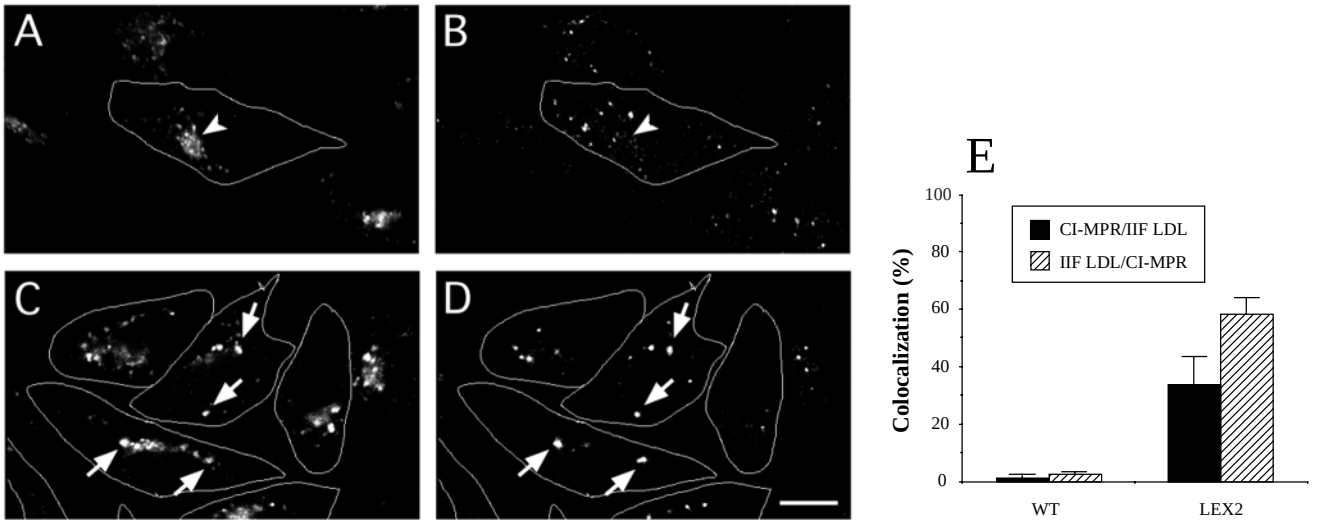

Fig. 6. Internalized LDL was transported to the CI-MPR-positive compartments in LEX2 cells. Wild-type cells (A,B) and LEX2 cells (C,D) internalized prebound unlabelled LDL for 20 minutes, and were then immunofluorescently double stained for CI-MPR (A,C) and LDL (B,D), using rabbit polyclonal anti-CI-MPR antibody and mouse monoclonal anti-human LDL IgG as primary antibodies. Arrowheads in A and B indicate the CI-MPR-positive, yet LDL-negative compartments. Arrows in C and D indicate the colocalization of CI-MPR and LDL. Cell profiles are drawn. Bar, 10 μm. (E) The colocalization of CI-MPR and internalized LDL was elevated in LEX2 cells. The extent of colocalization of CI-MPR and internalized LDL in wild-type (WT) and LEX2 cells in the same experiments as in A-D was analyzed semiquantitatively. The mean of data from four (WT) or five (LEX2) cells is shown. Bars indicate s.e.m.

LDL and CI-MPR was noticed also in wild-type and LEX1 cells transiently at 10 to 15 minutes of internalization, but only minor populations of both LDL and CI-MPR were found to be colocalized during this period (data not shown).

As previously mentioned, LEX2 cells exhibited the prominence of MVBs as observed by electron microscopy (Fig. 3A, mb). These MVBs in LEX2 cells were spherical and unusually well elaborated, and had a diameter of 0.4~1.3 μm. Such well-elaborated MVBs were hardly observed in wild-type cells. The increase in the larger MVBs in LEX2 cells was statistically significant (Student's *t*-test, $P<0.05$): the mean number of large MVBs (filled with internal vesicles, diameter >300 nm) per cell section (only that showing a cross section of the nucleus) in EM was 1.5±0.2 (s.e.m., $n=30$) in LEX2 cells, while no such large MVBs were observed in wild-type cells ($n=30$). Other membraneous organelles such as endoplasmic reticulum, the Golgi apparatus, and mitochondria appeared normal in LEX2 cells (Fig. 3A, and data not shown).

Immunoelectron microscopy revealed that the highly elaborated MVBs in LEX2 cells were positive for CI-MPR (Fig. 7A, arrow), showing that the MVBs correspond to the CI-MPR-positive dots observed by immunofluorescence. The CI-MPR-positive gold particles were observed mostly on the internal structures of the MVBs, rather than on the limiting outer membrane (Fig. 7A). This observation is consistent with previous reports on CI-MPR localization within MVBs (Killisch et al., 1992; Kobayashi et al., 1998b). Apart from these MVBs, large vacuoles containing filamentous materials with a size similar to that of the MVB were occasionally observed in LEX2 cells, and these vacuoles were mostly devoid of CI-MPR (Fig. 7A, arrowhead). Hence, endocytosed intact LDL was accumulated in the CI-MPR-positive MVBs in LEX2 cells. Immunoelectron microscopy for CI-MPR also confirmed the phenotypic difference between LEX2 cells and LEX1 cells: the perinuclearly aggregated late endosome/lysosome vesicles in LEX1 cells were mostly negative for CI-MPR (Fig. 7B).

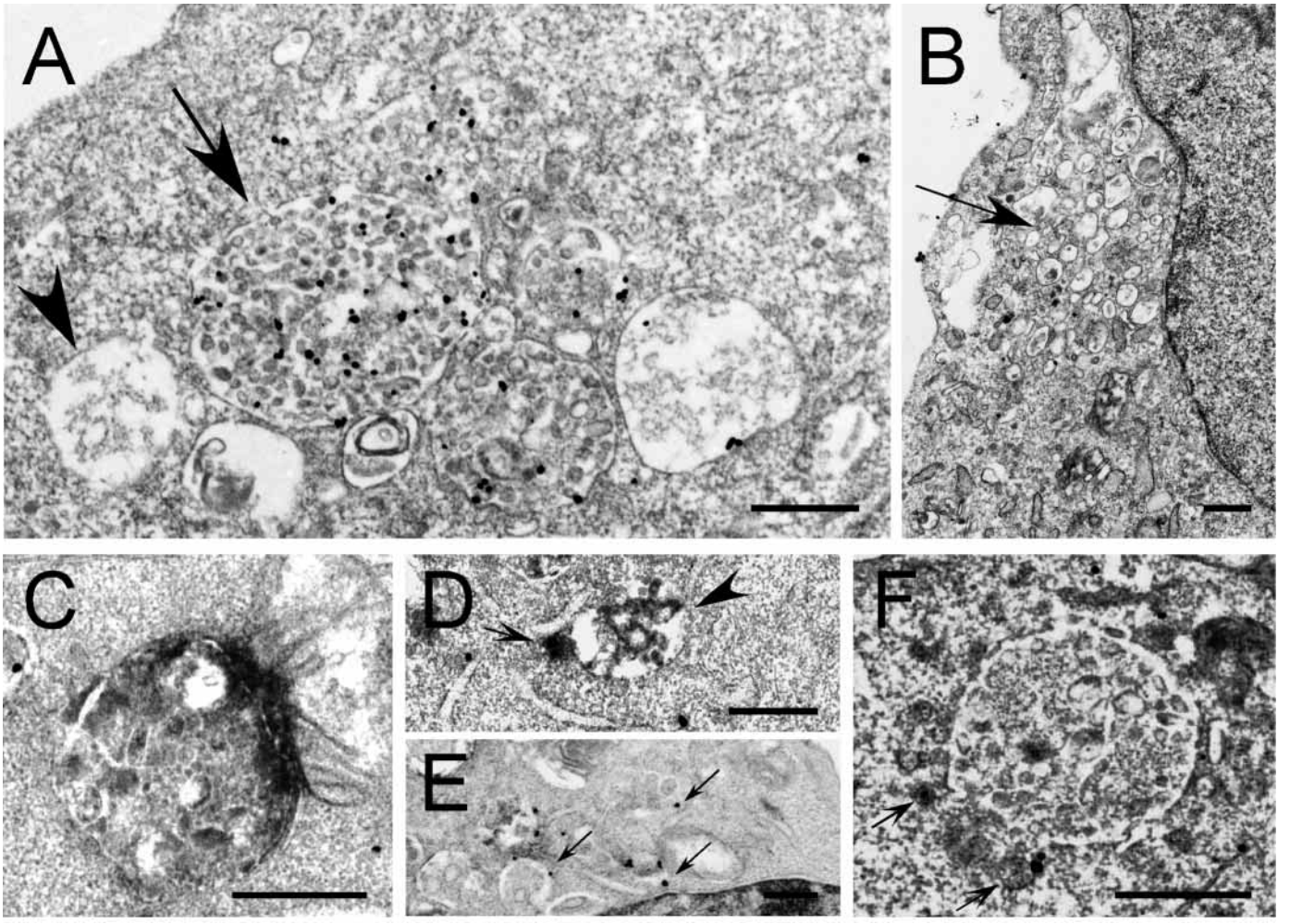

Fig. 7. The MVBs in LEX2 cells were positive for CI-MPR, yet negative for rab7. (A,B) Immunoelectron microscopic localization of CI-MPR in a LEX2 cell (A) and in a LEX1 cell (B). The arrow and the arrowhead in A indicate a CI-MPR-positive MVB and a CI-MPR-negative vacuole, respectively. The arrow in B indicates a perinuclear vesicle aggregate. (C,D) Double immunoelectron microscopic localization of rab7 (silver-enhanced gold particles) and lgp-B (HRP reaction products) in LEX2 cells. (C) An example of an lgp-B-positive MVB that was negative for rab7. (D) A rab7-positive smaller structure (arrow) adjacent to the lgp-B-positive MVB (arrowhead). (E) Examples of cytoplasmic rab7-positive structures including electron-lucent, lgp-B-negative profiles (arrows). (F) Immunoelectron microscopic localization of a constitutively active rab7 in a LEX2 cell. NHArab7Q67L was visualized using anti-HA epitope antibody in a LEX2 cell expressing this protein by retrovirus-mediated gene transfer. Arrows indicate NHArab7Q67L-positive vesicular structures adjacent to a large MVB. Bars, 500 nm.

Double immunolocalization of rab7 and lgp-B in LEX2 cells revealed that the body of the large MVBs positive for lgp-B was mostly devoid of rab7 (Fig. 7C,D). Small vesicles adjacent to MVBs were occasionally found to be positive for rab7 (Fig. 7D) or constitutively active NHArab7Q67L (Fig. 7F). Other more frequently observed cytoplasmic rab7-positive structures in LEX2 cells were not easy to identify, but included electron-lucent profiles negative for lgp-B (Fig. 7E).

Intermixing of contents between the MVBs was slow in LEX2 cells

In order to examine transport properties of the LEX2 MVBs, we analyzed the colocalization of two fluorescent LDLs internalized separately in LEX2 cells. The localization of endocytosed DiO-LDL (five-minute pulse, 93-minute chase) and R18-LDL (three-minute pulse, 60-minute chase) was analyzed by confocal microscopy in wild-type, LEX1, and LEX2 cells (Fig. 8A-I). From the aforementioned double localization experiments for LDL and CI-MPR, both of internalized fluorescent LDLs were expected to colocalize with CI-MPR in LEX2 cells at this time point. In wild-type and LEX1 cells, these two fluorescent LDLs were observed largely colocalized (Fig. 8A,B,D-G). In marked contrast, in LEX2 cells, these LDLs were observed in separate dots (Fig. 8C,H,I).

The time course of the intermixing of LDLs in similar experiments was studied semiquantitatively by examining the colocalization of DiO-LDL (five-minute pulse, 93-minute chase) and R18-LDL chased for various periods after a three-minute pulse uptake in wild-type, LEX1, and LEX2 cells (Fig. 8J,K). In wild-type cells, after a rapid rise, intermixing reached a plateau at about 30 minutes of R18-LDL chase (Fig. 8J,K). This time course suggests that, in wild-type cells, most LDL reached structures intermixing each other's contents quickly, or a common terminal station, presumably the lysosomes, at chase time of about 30 minutes. In LEX1 cells, intermixing of LDLs is slower than in wild-type cells (Fig. 8J,K). However, a continuous increase of intermixing was observed during the 60-minute chase time reaching the wild-type level at the end of the chase (Fig. 8J,K). This observation is consistent with our previous interpretation of the LEX1 phenotype that the equilibrium between LEX1 late endosomes and lysosomes is shifted towards the former from the latter due to retardation in the forward transport. By contrast, in LEX2 cells, the colocalization of the two fluorescent LDLs was lower than in the other cells at most time points (Fig. 8J,K). Furthermore, the intermixing in LEX2 cells seemed to be saturable at a lower level than in wild-type or LEX1 cells (Fig. 8J,K), suggesting that, once their formation is complete, the LEX2 compartments remain mutually isolated for a relatively long time.

The recycling pathway to the plasma membrane was normal in LEX2 cells

The recycling pathway of the LDL receptor was assessed as described previously (Ohashi et al., 1999) by measuring a 10-minute pulse uptake of DiO-LDL after uptakes of unlabeled LDL for various periods. The uptake of DiO-LDL was not reduced in LEX2 cells as compared with the case in wild-type cells even when preincubation with unlabelled LDL was performed (Fig. 9), indicating that LDL receptors are reused in LEX2 cells as efficiently as in wild-type cells. Moreover, the presence of monensin, known to inhibit the recycling of the LDL receptor (Basu et al., 1981), reduced the uptake of DiO-LDL in both wild-type and LEX2 cells (Fig. 9), indicating monensin interrupted receptor recycling also in LEX2 cells. These data suggest that the receptor recycling pathway is not perturbed in LEX2 cells.

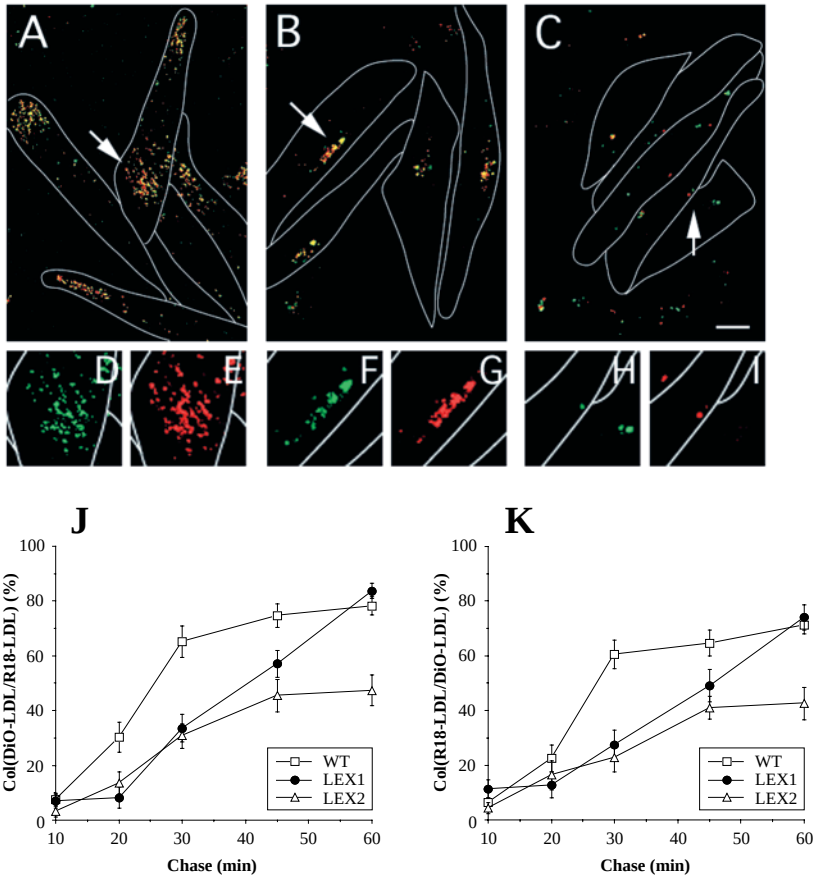

Fig. 8. Intermixing of contents between the MVBs was slow in LEX2 cells. (A-C) Wild-type cells (A), LEX1 cells (B), and LEX2 cells (C) internalized DiO-LDL (green) for five minutes, and were chased for 30 minutes at 37°C. Then the cells internalized R18-LDL (red) for three minutes at 37°C and were further chased for 60 minutes. The cells were subjected to confocal microscopy. Bar, 10 μm. (D,E), (F,G), and (H,I) Paired single-color higher magnification images of the parts indicated by arrows in A, B, and C, respectively. (J,K) Time course of the extent of colocalization between DiO-LDL and R18-LDL endocytosed separately. After DiO-LDL was internalized for five minutes, wild-type (WT), LEX1 (LEX1), and LEX2 cells (LEX2) were chased for 93 minutes at 37°C. During the chase, R18-LDL was internalized for three minutes at 37°C and chase incubations were performed for indicated times (Chase). The cells were subjected to confocal microscopy, and Col(DiO-LDL/R18-LDL) (J) and Col(R18-LDL/DiO-LDL) (K), indicating the extent of colocalization of DiO-LDL and R18-LDL, were calculated. The mean of data from four to 18 cells is shown. Bars indicate s.e.m.

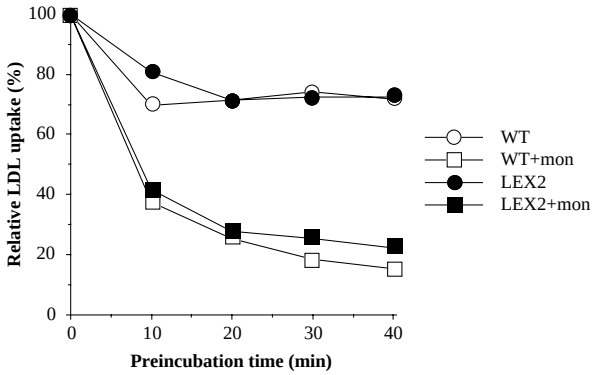

Fig. 9. LDL receptors recycled back to the plasma membrane normally in LEX2 cells. Wild type cells (WT) and LEX2 cells (LEX2) endocytosed 10 μg/ml unlabeled LDL for various times as indicated (Preincubation time). The cells were then washed, and received prewarmed (37°C) LPDS/F12 containing 10 μg/ml DiO-LDL, and were incubated for 10 minutes at 37°C. The same treatment was done in the presence of 25 μM monensin with wild-type cells (WT+mon) and LEX2 cells (LEX2+mon). The amount of endocytosed DiO-LDL was determined by flow cytometry and expressed as percentage of that at preincubation time zero.

DISCUSSION

Using a method that allowed mutant sorting based directly on the difference in the phenotype, we have established CHO cell mutants defective in lysosomal degradation of a fluorescent LDL. About 10^6 of individually mutagenized cells had been screened. The established mutants showed a variety of abnormal endocytic phenotypes. We have applied somatic cell genetics on these newly isolated mutants, and identified three complementation groups, one into which the previously isolated LEX1 mutant falls, and the other two showing novel defective features.

LEX2 cells are defective in the segregation and sequestration of contents at compartments equivalent to ECV/ maturing MVBs

One of the newly isolated mutants, LEX2, fell into complementation group B and exhibited a unique characteristic, the prominence of well-elaborated MVBs, hardly seen in wild-type cells. Several observations point to that these vesicles are the transport intermediates, previously referred to as ECVs or maturing MVBs, destined for late endosomes (reviewed by Gu and Gruenberg, 1999; Mukherjee et al., 1997). First, these vesicles were devoid of an early endosome marker, transferrin receptor, and a late endosome marker, rab7. Second, the vesicles were spherical, and were with typical multivesicular appearance for ECVs. The size of the LEX2 MVBs was relatively large (0.4~1.3 μm), in an overlapping but somewhat larger size range than that reported for the ECVs (0.4~0.7 μm; Gruenberg et al., 1989). The larger size may reflect the accumulation of materials within the MVBs due to their functional perturbation (see below). Third, inclusion of endocytosed LDL into these vesicles started at 10-15 minutes of internalization and was complete at ~20 minutes, a comparable time course that was reported for BHK cells in which endocytosed vesicular stomatitis virus G protein was observed in ECVs between 5 and 15 minutes of internalization (Gruenberg et al., 1989). In addition, intermixing kinetics of LDLs endocytosed separately suggested that the content exchange between the LEX2 MVBs was relatively slow and saturable at a much lower level than that observed between wild-type or LEX1 late endosomes/lysosomes (Fig. 8). This suggested that, once their formation is complete, LEX2 MVBs remain mutually isolated for a relatively long time. In cell-free fusion experiments, it was previously shown that the ECVs have relatively little fusion activity with each other, while late endosomes share with the early endosomes a high capacity to undergo homotypic fusion (Aniento et al., 1993; Gruenberg and Howell, 1989). Hence, the property of LEX2 MVBs is consistent with their being equivalents of ECVs with a relatively low mutual fusion activity, rather than their being early or late endosomes. To our knowledge, LEX2 mutant is the first CHO mutant exhibiting ECV-like MVBs as a possible arrested intermediate.

The MVBs observed in LEX2 cells were positive for lgp-B and CI-MPR and an MPR ligand, cathepsin D. Endocytosed LDL reached the CI-MPR-positive MVBs rapidly, but stayed longer (up to ~90 minutes of uptake) with CI-MPR before any separation was observed. The accumulation of these proteins within LEX2 MVBs can be explained by direct impact of the LEX2 gene defect upon ECV/MVB functions. Unlike rab7, which cycles between cytosol and the membrane with which the active rab7 associates, lgp-B and CI-MPR (plus its ligands including cathepsin D) will transit ECVs during their itinerary to late endosomes/lysosomes from early endosomes: The earliest point of convergence of the lysosomal biosynthetic and the endocytic pathways is the early endosome, and it is likely that the MPRs and their ligands follow the classical endocytic pathway, taken by endocytosed LDL, from early to late endosomes (Hoflack and Lobel, 1993; Ludwig et al., 1991). In rat hepatocytes, a significant fraction of newly synthesized lgp-B is delivered to lysosomes by way of early endosomes (Akasaki et al., 1996). It might also be possible that the ECV/MVBs themselves are capable of receiving CI-MPR (and possibly lgps) from the TGN at least at their early stage as suggested in HEp-2 cells (Hirst et al., 1998). Hence, a direct impact on ECV/MVB functioning in sorting or export of CI-MPR, lgp-B, and endocytosed LDL to their correct destinations will result in the accumulation of these incoming proteins within the ECV/maturing MVBs.

Such an impact on sorting and export functioning of ECV/MVBs would result in retarded ECV/MVB consumption. Retarded ECV/MVB consumption can explain the higher frequency and the better elaboration of MVBs observed in LEX2 cells, since the balance between the formation/ elaboration and the consumption of ECV/MVBs would determine the steady-state frequency and the complexity of ECV/MVBs: With retarded ECV/MVB consumption, (i) more of MVBs are formed de novo before preexisting MVBs are consumed, and (ii) there would be a longer time for the elaboration of a preexisting MVB. Perhaps in wild-type CHO cells, ECV/MVB consumption is so rapid that large well-elaborated MVBs as observed in LEX2 cells are hardly seen in the steady state.

LEX1 and LEX2 mutations dissect distinct late endocytic stages

LEX1 and LEX2 cells fell into different complementation

groups, suggesting the involvement of two separate genes in the observed impaired phenotypes in these mutants. In agreement with this, the arrested point of LEX2 cells was clearly distinct from that of LEX1 cells: The perinuclear heterogeneous late endosome/lysosome aggregate characteristic of LEX1 cells (Ohashi et al., 1999) was not observed in LEX2 cells. In addition, there was elevated colocalization of rab7 with lgp-positive vesicles in LEX1 cells but not in LEX2 cells, suggesting that rab7-positive late endosomes are not involved in the defective MVB stage in LEX2 cells. At the same time, the observation is consistent with the previous interpretation that, in LEX1 cells, the equilibrium is shifted towards late endosomes from the lysosomes (thus resulting in more of rab7-positive endosomes; Ohashi et al., 1999), and the previously postulated role of rab7 in the direct interaction between late endosomes and lysosomes, rather than in earlier endosomes (Ohashi et al., 1999). By contrast, CI-MPR was redistributed from the Golgi pattern to the MVBs in LEX2 cells, but not in LEX1 cells. Thus, the CI-MPR sorting stage at late endosomes does not seem to be affected in LEX1 cells. Taken together, LEX2 cells are likely to be defective in the following possibly coupled stages: (1) the protein sorting stage in the ECV/MVBs, and (2) the process from the ECV/MVBs to the post-sorting, rab7-positive, lysosome-interacting late endosomes.

Nevertheless, it might be possible that phenotypically distinctive arrested structures observed in LEX1 and LEX2 cells do not represent two successive stages, but two extreme forms of a compartment with multiple functions, aberrantly induced by one or the other of the mutations. However, in LEX2 cells, there seem to be rab7-positive structures in the wild-type distribution, distinct from the arrested ECV/MVBs, suggesting the separate identity of the rab7 structures even in the arrested state of LEX2 cells. While future works are required to elucidate the nature of these rab7-positive structures, they could be remnants or minimum core structures of the rab7-positive normal late endosomes. Furthermore, a couple of lines of evidence suggest that the LEX2 defective stage is earlier than the LEX1 arrested stage. First, endocytosed LDL started appearing in the CI-MPR-positive MVBs at 10-15 minutes of internalization in LEX2 cells, whereas it took ~30 minutes for LDL to reach the unusual perinuclear aggregate of late endosomes and lysosomes in LEX1 cells (Ohashi et al., 1999). The colocalization of endocytosed LDL and CI-MPR was noticed also in wild-type and LEX1 cells transiently at 10 to 15 minutes of internalization, but only minor populations of both LDL and CI-MPR were found to be colocalized during this period. These observations suggest the existence of a CI-MPR-positive stage before the LEX1 arrested late endosomes, and this stage prolonged in LEX2 cells. Second, RET-LDL degradation in LEX2 cells was significantly slower than in LEX1 cells, and the antigenicity of endocytosed LDL was well preserved in the arrested rab7-negative, ECV-like MVB in LEX2 cells as shown by immunolocalization of LDL. Thus, the MVB in LEX2 cells appears to be a non-digestive compartment. In contrast, the fact that LEX1 rab7-positive structures were hydrolytic to some extent suggested that they are late endosomes with digestive activities (Ohashi et al., 1999). These observations imply that the LEX2 MVBs are earlier, premature, less-digestive endosomes as compared with LEX1 arrested late endosomes, and that the transition

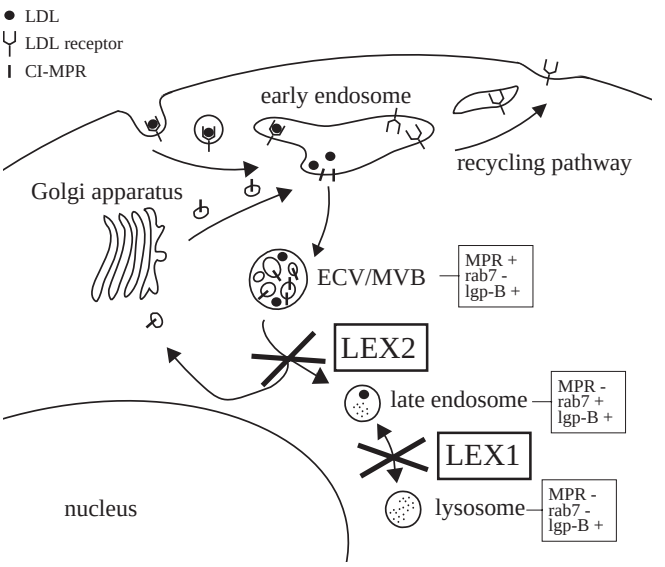

Fig. 10. A model for distinct late endocytic stages in CHO cells dissected by LEX1 and LEX2 mutations. LEX1 and LEX2 mutants have implied the existence of two separable stages in the late endocytic pathway in CHO cells: (1) sorting of proteins within the ECV/MVBs possibly coupled with consumption of the ECV/MVBs, and (2) direct interaction between rab7-positive late endosomes and the lysosomes. For details, see the text.

from the MVBs to a later rab7-positive, lysosome-interacting stage would be important for lysosomal digestive functions. At present, however, it is unclear whether such transition includes fusion between the MVB and the rab7-positive endosomes, or the MVB can mature into a fusion-competent, rab7-positive state. LEX1 and LEX2 mutations could be considered as landmarks for these late endocytic stages (Fig. 10), and use of these cells in further study would help to clarify the exact order of events taking place.

Conclusions

The importance of MVBs has been implicated in a number of physiological processes such as axonal transport and exosome biogenesis (Gu and Gruenberg, 1999; Parton et al., 1992; Thery et al., 1999). ECV/MVB dynamics may provide efficient mechanisms for packaging and transporting specific membranes and cytosolic components for specialized purposes. The unique construction of MVBs has attracted much attention concerning their structure-function relationships, which remain to be clarified. The presently established mutants had shown various phenotypes. For example, LEX2 and the other group B cells exhibited the vacuole/MVBs showing various degrees of elaboration with a rather continuous spectrum. Comparative phenotypic studies together with the identification and manipulation of gene defects of the presently established mutants would help to investigate the mechanism of late endosome dynamics such as formation, elaboration, and consumption of MVBs and their relationship to later endosomes connected to lysosomes. The repeated flow-cytometric sorting method used here to isolate the mutants would be useful also for the identification of gene defects by expression cloning, for which techniques that allow the isolation of revertants are essential.

APPENDIX

Simulating and monitoring mutant isolation by repeated flow-cytometric cell sorting based on theoretical consideration

Introduction

The feasibility of flow-cytometric mutant selection is largely a question of how a rare mutant cell of one's interest can be separated from the huge population of surrounding 'wild-type' cells. A rare mutant cell could be only one one-millionth of the population of mutagenized cells. Analyzing and selecting a cell population at such a low frequency is not an easy task (Leary, 1994). Mutant selection should be done with reasonably high selection efficiency, screening a sufficiently large number of cells.

In the following sections, we consider the repeated flow-cytometric sorting process theoretically and simulate the whole process based on the theoretical consideration in order to set up an efficient strategy. Then we perform mutant screening in accordance with the simulation, and monitor the screening process to evaluate the efficiency of each round of cell sorting.

Theory

Definitions

The parameters used are defined as follows. A: the number of initially mutagenized cells. B: the number of expected mutant clones included in the initially mutagenized cells. R: the number of the round of FACS sorting. Nap_R: the number of cells subjected to the round R of FACS sorting. N_R: the number of selected cells in the round R of FACS sorting. n_R: times of multiplication of cells between the round numbers (R-1) and R of FACS sorting. w_R, m_R: yields of wild-type cells and mutants, respectively, with a set sorting region (or window) in the round R of FACS sorting. $d(W)_R$, $d(M)_R$: probabilities of completely losing a clone of wild-type cells and a clone of mutant cells, respectively, in the round R of FACS sorting. $E(W)_R$, $E(M)_R$: expectations of the number of cells derived from a clone of wild-type cells and a clone of mutant cells, respectively, after the round R of FACS sorting.

Calculation of $d(W)_R$, $d(M)_R$, $E(W)_R$, and $E(M)_R$

Assume that mutagenized clonal cells are cultured to give uniform n_1 times multiplication before the first FACS sorting. Thus n_1 cells of each clone are present. If, during the first sorting with a selected window setting, cells belonging to clone X (clone X cells) are retrieved with a yield, y_1, the probability of the number (designated as k) of recovered clone X cells distributes binomially:

$$P(k)_1 = {}_{n_1}C_k y_1^k (1 - y_1)^{n_1 - k}, \quad k = 0, 1, 2, ..., n_1 .$$

Hence, the probability of completely losing clone X cells in the first sorting is given as.

$$d_1 = P(0)_1 = (1 - y_1)^{n_1} .$$

Here the expectation of the number of cells derived from clone X is $E_1 = n_1 y_1$.

In the second sorting, the retrieved cells are cultured to give n_2 times multiplication before sorted by cell sorter. Thus n_2 cells of each retrieved are present. If clone X cells were not completely lost during the first sorting, the probability distribution of the number (k) of clone X cells just before the second sorting is given as follows:

$$P(k) = \frac{{}_{n_1}C_l y_1^l (1 - y_1)^{n_1 - l}}{1 - (1 - y_1)^{n_1}}, \quad k = n_2 l; \quad l = 1, 2, ..., n_1 .$$

Assume that clone X cells are recovered with yield y_2 in the second sorting. With each $k(=n_2 l)$, the probability of the number of recovered cells in the second sorting distributes binomially. Therefore, the probability of completely losing clone X cells upon the second sorting is calculated as:

$$d_2 = \frac{[y_1(1 - y_2)^{n_2} + (1 - y_1)]^{n_1} - (1 - y_1)^{n_1}}{1 - d_1} .$$

Here the expectation of the number of cells derived from clone X is calculated as:

$$E_2 = \frac{n_1 y_1 n_2 y_2}{1 - d_1} .$$

Likewise, by inductive calculation, the probability of completely losing clone X cells in sorting round R is calculated as:

$$d_R = \frac{\left(\langle\{...[(1-y_R)^{n_R}y_{R-1}+1-y_{R-1}]^{n_{R-1}}y_{R-2}+...\}^{n_3}y_2+1-y_2\rangle^{n_2}y_1+1-y_1\right)^{n_1}-\sum_{k=1}^{R-1}q_k}{\prod_{k=1}^{R-1}(1-d_k)},$$

where q_k is the numerator part of d_k.

Using this equation, we obtain:

$$d(W)_R = \frac{\left(\langle\{...[(1-w_R)^{n_R}w_{R-1}+1-w_{R-1}]^{n_{R-1}}w_{R-2}+...\}^{n_3}w_2+1-w_2\rangle^{n_2}w_1+1-w_1\right)^{n_1}-\sum_{k=1}^{R-1}q(W)_k}{\prod_{k=1}^{R-1}[1-d(W)_k]}$$

and

$$d(M)_R = \frac{\left(\langle\{...[(1-m_R)^{n_r}m_{R-1}+1-m_{R-1}]^{n_{R-1}}m_{R-2}+...\}^{n_3}m_2+1-m_2\rangle^{n_2}m_1+1-m_1\right)^{n_1}-\sum_{k=1}^{R-1}q(M)_k}{\prod_{k=1}^{R-1}[1-d(M)_k]}$$

The expectation of the number of cells derived from clone X is calculated as:

$$E_R = \frac{\prod_{k=1}^{R}n_k y_k}{\prod_{k=1}^{R-1}(1-d_k)}.$$

Thus,

$$E(W)_R = \frac{\prod_{k=1}^{R}n_k w_k}{\prod_{k=1}^{R-1}[1-d(W)_k]}$$

and

$$E(M)_R = \frac{\prod_{k=1}^{R}n_k m_k}{\prod_{k=1}^{R-1}[1-d(M)_k]}.$$

Criteria for choosing a FACS sorting window

Two criteria for choosing a FACS sorting window (or a region) were set: (1) The value m_R/w_R, selectivity for mutant cells over wild-type cells, should be the maximum in order to efficiently concentrate mutant cells over wild-type cells. (2) the value $1-d(M)_R$ should be the largest (as close to unity as possible) in order to cover the largest possible net population of screened mutagenized cells. The latter criterion is set because, after FACS sorting round R, mutant cells that had been present in the initial

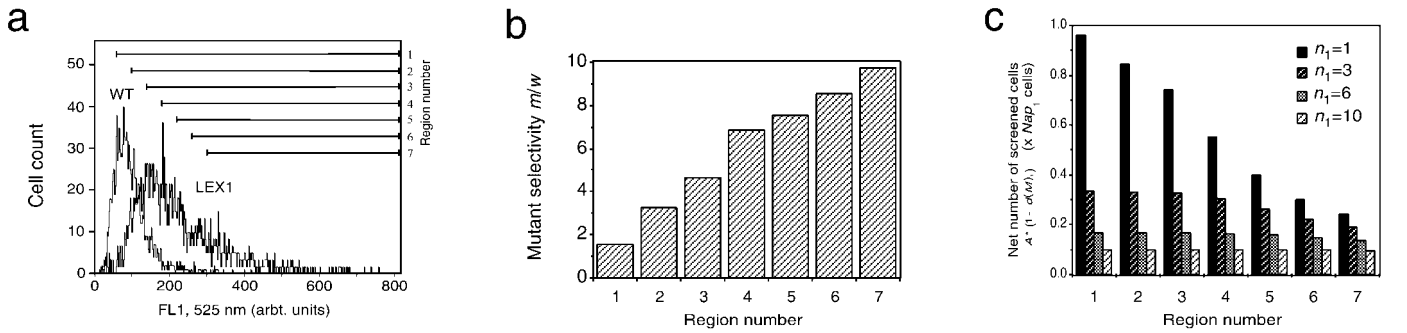

Fig. 1. The choice of a sorting region for mutant screening by flow-cytometric cell sorting using NBD-LDL. Essentially the same procedure was done for the choice of a sorting window for screening using RET-LDL. (a) Flow-cytometric analysis of wild-type and LEX1 cells that endocytosed NBD-LDL in a pulse-chase experiment. Wild-type (WT) and LEX1 cells (LEX1) endocytosed NBD-LDL (10 μg/ml) in a 10-minute pulse. Then chase incubation was performed for 100 minutes. The cells were then removed from the dishes and were subjected to analytical flow cytometry for NBD fluorescence. Three thousand cells were analyzed. Mutant sorting regions (bars) numbered 1-7 (region number) were tentatively set on the histograms. (b) Mutant selectivity with each tentative sorting region. Yields of LEX1 cells (*m*) and wild-type cells (*w*) with regions 1-7 (region number) in a were obtained as fractions of LEX1 cells and wild-type cells, respectively, included in the particular region. From these values, mutant selectivity (*m*/*w*) was calculated. (c) The net number of screened cells after the first screening using sorting regions 1-7 (region number) indicated in a. The number $A^*(1-d(M)_1)=(Nap_1/n_1)^*(1-(1-m_1)^{n_1})$, as the function of n_1 at fixed Nap_1, was calculated using *m* obtained in b, and is expressed relative to Nap_1.

$A^*\prod_{k=1}^{R}(1-d(M)_k)$ of mutagenized cells were expected to have survived; hence, the net number of screened mutagenized cells is estimated as $A^*\prod_{k=1}^{R}(1-d(M)_k)$. In reality, these two criteria are mutually exclusive. Thus the most adequate window setting for a given requirement (either for better selectivity for late stages of screening, or for a larger number of screened cells for initial stages of screening, see below) was chosen.

On the other hand, $A^*\prod_{k=1}^{R}(1-d(W)_k)$ indicates the maximum clonal number of wild-type cells still remaining after FACS sorting round *R*. Thus, when the number $A^*\prod_{k=1}^{R}(1-d(W)_k)$ had become less than one, sorting was expected to be enough repeated.

Simulation of the mutant sorting process

The sorting process was simulated by calculating the net number of screened mutagenized cells ($A^*\prod_{k=1}^{R}(1-d(M)_k)$) and the maximum clonal number of survived wild-type cells ($A^*\prod_{k=1}^{R}(1-d(W)_k)$) at each round of sorting, assuming the values *A*, *B*, Nap_R, w_R and m_R. Value Nap_R was assumed considering the FACS performance (see below). Value *A* was calculated as $A=Nap_1/n_1$, where n_1 is the required number of doublings of mutagenized cells for fixation and expression of induced mutation (see below). Parameters w_R and m_R were set according to the results of reference FACS analyses of wild-type cells and previously isolated reference mutant cells (LEX1 cells), using various sorting regions (or windows) as described below. The number of selected cells in sorting round *R* was estimated by the equation: $N_R=(A-B)^*E(W)_R+B^*E(M)_R$. The selected cells were assumed to have been cultivated until the cell number reached Nap_R, and the whole grown cell population subjected to the next round of sorting. The multiplication of selected cells is then calculated as $n_R=Nap_R/N_{R-1}$.

In practice, we assumed use of NBD-LDL and RET-LDL. These LDLs give different advantages. The principle of the use of NBD-LDL is based on fluorescence measurement at a single wavelength. The fluorescence intensity is dependent on the amount of endocytic uptake of NBD-LDL, and on the processing of NBD after the degradation of NBD-LDL in lysosomes. In contrast,

Table 1. A simulation of the mutant sorting process

Sorting round no. (*R*)	No. of previously selected cells (N_{R-1})	No. of applied cells (Nap_R)	n_R	m_R	$1-d(M)_R$	$A^*\prod_{k=1}^{R}(1-d(M)_k)$	w_R	$1-d(W)_R$	$A^*\prod_{k=1}^{R}(1-d(M)_k)$
1	1,000,000*	3,000,000	3	0.5	0.88	880,000	0.08	0.22	220,000
2	240,000	3,000,000	12	0.2	0.97	850,000	0.02	0.24	53,000
3	60,000	3,000,000	50	0.2	1.0	850,000	0.02	0.67	35,000
4	60,000	2,000,000	33	0.02	1.0	850,000	0.0004	0.022	790
5	930	2,000,000	2200	0.02	1.0	850,000	0.0004	0.58	460
6	6,400	2,000,000	310	0.02	1.0	850,000	0.0004	0.17	76
7	36,000	2,000,000	56	0.02	1.0	850,000	0.0004	0.025	1.9
8	40,000	2,000,000	50	0.02	1.0	850,000	0.0004	0.020	0.040

*Mutant selection was started with 1,000,000 (=*A*) mutagenized cells that were assumed to contain five (=*B*) independent clonal mutant cells with a LEX1-like phenotype. Repeated FACS sorting was assumed to be done as described in the text, first three times with NBD-LDL and thereafter with RET-LDL. The selection process was simulated by calculating the indicated parameters. n_R, multiplication of cells; m_R, yield of LEX1-like mutant cells; $d(M)_R$, probability of losing a LEX1-like mutant clone; $A^*\prod_{k=1}^{R}(1-d(M)_k)$, net number of screened mutagenized cells; w_R, yield of wild-type cells; $d(W)_R$, probability of losing a wild-type clone; $A^*\prod_{k=1}^{R}(1-d(W)_k)$, maximum clonal number of survived wild-type cells. For details of calculation, see the text.

the RET-LDL method is more specific as to the detection of lysosomal degradation, since the degradation analysis can be done independently of the amount of the endocytic uptake and is susceptible to the early phase lysosomal degradation (Ohashi et al., 1992). However, NBD-LDL could give at the same selectivity a smaller probability of losing a clone of mutant cells ($d(M)_R$). Since the number of cells derived from one mutant clone is expected to be lower at initial rounds of sorting than at later stages with a finite *Nap*, the loss of the net size of screened cells is a larger problem at the early rounds of sorting. Hence, to keep the net size of screened cells large, NBD-LDL, providing a small $d(M)_R$, rather than RET-LDL was chosen for initial three rounds of screening. As this problem gets less significant with increasing rounds of sorting, more specific RET-LDL was employed at later sorting stages.

The choice of a sorting window (or region) also affects the selectivity for mutant cells over wild-type cells (m/w), and the probabilities of losing completely a clone of wild-type cells and a clone of mutant cells ($d(W)$, $d(M)$, respectively). Sorting windows and regions were selected as follows: In reference experiments, wild-type cells and LEX1 mutant cells were analyzed by flow cytometry in a pulse-chase format (Fig.1a). In a FACS analysis histogram, various sorting regions (or windows) were set (Fig. 1a) and m and w with each region obtained as fractions of LEX1 cells and wild-type cells, respectively, included in the particular region. From these values, mutant selectivity (m/w) and the net number of screened cells $A^*\prod(1-d(M))$ were calculated with each region (Fig. 1b,c). A region that gives sufficient mutant selectivity at the same time a reasonable net number of screened cells (e.g. region 4 in Fig. 1b,c with n_1=3; for n_1 determination, see below) was chosen.

The net size of screened cells, $A^*\prod_{k=1}^{R}(1-d(M)_k)$, is dependent also on n_R. This value was automatically estimated for $R\geq 2$ as described in the Theory section. However, n_1, the multiplication number of mutagenized cells before the first FACS screening, needed to be determined so that the net size of screened mutagenized cells after the first sorting is kept the maximum. From the consideration in Theory, the net number of screened cells after the first sorting was estimated as:

$$A^*[1-d(M)_1] = \frac{Nap_1}{n_1} *[1-(1-m_1)^{n_1}] .$$

The dependency of this value on n_1 is also shown in Fig. 1c. The results indicated that n_1 should be kept to the practical minimum. Thus the minimum number of cell doublings required for the fixation and expression of the induced mutation (in general, three to five doublings; Gargus, 1989) should be employed as n_1. In an example of simulation shown in Table 1, we used n_1=3.

Using these selected settings, the whole process of mutant screening was simulated (Table 1). A frequency of 10^{-6}~10^{-5} of expected mutant cells (in this case, five (=B) LEX1-like mutants in 1,000,000 (=A) mutagenized cells) was assumed. Two to three millions (Nap_R) of cells were assumed to be subjected to each round of sorting so that each flow-cytometric sorting process could be done within a couple of tens of minutes by the FACS Vantage system. As the result of simulation, it was estimated that, after seven to eight rounds of FACS sorting, we would be able to obtain a mutant cell pool ($A^*\prod_{k=1}^{8}(1-d(W)_k)<1$), having screened a net number of 8.5×10^5 mutagenized cells ($=A^*\prod_{k=1}^{8}(1-d(M)_k)$). The obtained pool was expected to contain about 4.3 ($=B^*\prod_{k=1}^{8}(1-d(M)_k)$) independent mutant clones out of initial five, while expected to contain much less than one ($(A-B)^*\prod_{k=1}^{8}(1-d(W)_k)$) of wild-type clones. Such calculation was done also at other mutant frequencies. For example, with B values of 100 and 1,000, FACS sorting rounds of seven and six times, respectively, were estimated to be sufficient to obtain mutant pools containing 85% of initial mutant clones. These results indicated that mutant cells at a frequency of 10^{-6}~10^{-3} could be isolated by six to eight times of repetition of flow-cytometric cell sorting.

Monitoring the mutant sorting process

The net number of screened mutagenized cells ($A^*\prod_{k=1}^{R}(1-d(M)_k)$) and the maximum clonal number of survived wild-type cells ($A^*\prod_{k=1}^{R}(1-d(W)_k)$) at each round of sorting were calculated to evaluate each round of FACS sorting. Actual values of A, N_R, Nap_R, m_R and w_R were experimentally determined and were used in the calculation.

An example of monitoring the sorting process of a set of cells is shown in Table 2. After three rounds of sorting with NBD-LDL and subsequent four rounds with RET-LDL, the value $A^*\prod_{k=1}^{7}(1-d(W)_k)$ became less than one, indicating sorting had been sufficiently repeated (Table 2). Indeed, at this point, the cell pool showed slowed RET-LDL disintegration. It was estimated that 2.5×10^5 cells (net) have been screened (Table 2, $A^*\prod_{k=1}^{7}(1-d(M)_k)$).

Table. 2. An example of monitoring the mutant sorting process

Sorting round no. (R)	No. of previously selected cells (N_{R-1})	No. of applied cells (Nap_R)	n_R	m_R	$1-d(M)_R$	$A^*\prod_{k=1}^{R}(1-d(M)_k)$	w_R	$1-d(W)_R$	$A^*\prod_{k=1}^{R}(1-d(M)_k)$
1	1,500,000*	2,700,000	1.8	0.19	0.32	470,000	0.025	0.05	67,000
2	350,000	3,700,000	11	0.12	0.76	360,000	0.02	0.20	13,000
3	120,000	4,500,000	39	0.07	0.97	350,000	0.0075	0.27	3,600
4	170,000	2,100,000	12	0.025	0.71	250,000	0.00035	0.0050	20
5	2,800	1,300,000	470	0.018	1.0	250,000	0.0006	0.25	5
6	4,500	4,200,000	930	0.01	1.0	250,000	0.00095	0.62	3
7	18,000	3,000,000	170	0.006	1.0	250,000	0.0005	0.13	0.4

*Mutant selection was started with 1,500,000 mutagenized cells. Repeated FACS sorting was done as described in the text, first three times with NBD-LDL and thereafter with RET-LDL. The selection process was monitored by calculating the indicated parameters. n_R, multiplication of cells; m_R, yield of LEX1-like mutant cells; $d(M)_R$, probability of losing a LEX1-like mutant clone; $A^*\prod_{k=1}^{R}(1-d(M)_k)$, net number of screened mutagenized cells; w_R, yield of wild-type cells; $d(W)_R$, probability of losing a wild-type clone; $A^*\prod_{k=1}^{R}(1-d(W)_k)$, maximum clonal number of survived wild-type cells. For details of calculation, see the text.

We thank Dr Keiji Imoto (National Institute for physiological Sciences) for helpful advice and help in biochemistry. We also thank Dr Bruce Granger (Montana State University) and Dr Kazumi Ishidoh (Juntendo University) for providing us with antibodies, and Dr Hisataka Sabe (Osaka Bioscience Institute) for pBabe-puro. We are indebted to Ms Hiromi Akita for help in the operation of the FACS Vantage system, and Ms Masako Naruse, Mr Hiroshi Okawara, and Mr Masahiro Takagi for maintaining the cell-culture and cell-stock facilities. Analytical flow cytometry was done in NIBB center for Analytical Instruments. This work was supported in part by a Grant-in-Aid for Encouragement of Young Scientists from the Ministry of Education, Science, Sports and Culture of Japan (M.O.), and by the joint research program of the graduate university for advanced studies (M.O., A.Y. and K.N.).

REFERENCES

Advani, R. J., Yang, B., Prekeris, R., Lee, K. C., Klumperman, J. and Scheller, R. H. (1999). VAMP-7 mediates vesicular transport from endosomes to lysosomes. *J. Cell Biol.* **146**, 765-776.

Akasaki, K., Michihara, A., Fujiwara, Y., Mibuka, K. and Tsuji, H. (1996). Biosynthetic transport of a major lysosome-associated membrane glycoprotein 2, Lamp-2: a significant fraction of newly synthesized lamp-2 is delivered to lysosomes by way of early endosomes. *J. Biochem.* **120**, 1088-1094.

Aniento, F., Emans, N., Griffiths, G. and Gruenberg, J. (1993). Cytoplasmic dynein-dependent vesicular transport from early to late endosomes. *J. Cell Biol.* **123**, 1373-1387.

Basu, S. K., Goldstein, J. L., Anderson, R. G. and Brown, M. S. (1981). Monensin interrupts the recycling of low density lipoprotein receptors in human fibroblasts. *Cell* **24**, 493-502.

Bock, J. B., Klumperman, J., Davanger, S. and Scheller, R. H. (1997). Syntaxin 6 functions in trans-Golgi network vesicle trafficking. *Mol. Biol. Cell* **8**, 1261-1271.

Bomsel, M., Parton, R., Kuznetsov, S. A., Schroer, T. A. and Gruenberg, J. (1990). Microtubule- and motor-dependent fusion in vitro between apical and basolateral endocytic vesicles from MDCK cells. *Cell* **62**, 719-731.

Bright, N. A., Reaves, B. J., Mullock, B. M. and Luzio, J. P. (1997). Dense core lysosomes can fuse with late endosomes and are re-formed from the resultant hybrid organelles. *J. Cell Sci.* **110**, 2027-2740.

Brown, W. J. and Farquhar, M. G. (1987). The distribution of 215-kilodalton mannose 6-phosphate receptors within cis (heavy) and trans (light) Golgi subfractions varies in different cell types. *Proc. Nat. Acad. Sci. USA* **84**, 9001-9005.

Chavrier, P., Parton, R. G., Hauri, H. P., Simons, K. and Zerial, M. (1990). Localization of low molecular weight GTP binding proteins to exocytic and endocytic compartments. *Cell* **62**, 317-329.

Futter, C. E., Pearse, A., Hewlett, L. J. and Hopkins, C. R. (1996). Multivesicular endosomes containing internalized EGF-EGF receptor complexes mature and then fuse directly with lysosomes. *J. Cell Biol.* **132**, 1011-1023.

Gargus, J. J. (1989). Somatic cell mutants. In *Functional Epithelial Cells in Culture*, vol. 8 (ed. K. S. Matlin and L. D. Valentich), pp. 325-359. New York: Alan R. Liss, Inc.

Griffiths, G., Hoflack, B., Simons, K., Mellman, I. and Kornfeld, S. (1988). The mannose 6-phosphate receptor and the biogenesis of lysosomes. *Cell* **52**, 329-341.

Gruenberg, J. and Howell, K. E. (1989). Membrane traffic in endocytosis: Insights from cell-free assays. *Annu. Rev. Cell Biol.* **5**, 453-481.

Gruenberg, J., Griffiths, G. and Howell, K. E. (1989). Characterization of the early endosome and putative endocytic carrier vesicles in vivo and with an assay of vesicle fusion in vitro. *J. Cell Biol.* **108**, 1301-1316.

Gruenberg, J. and Maxfield, F. R. (1995). Membrane transport in the endocytic pathway. *Curr. Opin. Cell Biol.* **7**, 552-563.

Gu, F. and Gruenberg, J. (1999). Biogenesis of transport intermediates in the endocytic pathway. *FEBS Lett.* **452**, 61-66.

Haas, A., Scheglmann, D., Lazar, T., Gallwitz, D. and Wickner, W. (1995). The GTPase Ypt7p of *Saccharomyces cerevisiae* is required on both partner vacuoles for the homotypic fusion step of vacuole inheritance. *EMBO J.* **14**, 5258-5270.

Hirst, J., Futter, C. E. and Hopkins, C. R. (1998). The kinetics of mannose 6-phosphate receptor trafficking in the endocytic pathway in HEp-2 cells: the receptor enters and rapidly leaves multivesicular endosomes without accumulating in a prelysosomal compartment. *Mol. Biol. Cell* **9**, 809-816.

Hoflack, B. and Lobel, P. (1993). Functions of the mannose 6-phosphate receptors. *Advan. Cell Mol. Biol. Membr.* **1**, 51-80.

Imai, Y., Matsushima, Y., Sugimura, T. and Terada, M. (1991). A simple and rapid method for generating a deletion by PCR. *Nucl. Acids Res.* **19**, 2785.

Killisch, I., Steinlein, P., Romisch, K., Hollinshead, R., Beug, H. and Griffiths, G. (1992). Characterization of early and late endocytic compartments of the transferrin cycle. Transferrin receptor antibody blocks erythroid differentiation by trapping the receptor in the early endosome. *J. Cell Sci.* **103**, 211-232.

Kitamura, T., Onishi, M., Kinoshita, S., Shibuya, A., Miyajima, A. and Nolan, G. P. (1995). Efficient screening of retroviral cDNA expression libraries. *Proc. Nat. Acad. Sci. USA* **92**, 9146-9150.

Kobayashi, T., Gu, F. and Gruenberg, J. (1998a). Lipids, lipid domains and lipid-protein interactions in endocytic membrane traffic. *Semin. Cell Dev. Biol.* **9**, 517-526.

Kobayashi, T., Stang, E., Fang, K. S., de Moerloose, P., Parton, R. G. and Gruenberg, J. (1998b). A lipid associated with the antiphospholipid syndrome regulates endosome structure and function. *Nature* **392**, 193-197.

Kobayashi, T., Beuchat, M.-H., Lindsay, M., Frias, S., Palmiter, R. D., Sakuraba, H., Parton, R. G. and Gruenberg, J. (1999). Late endosomal membranes rich in lysobisphosphatidic acid regulate cholesterol transport. *Nature Cell Biol.* **1**, 113-118.

Leary, J. F. (1994). Strategies for rare cell detection and isolation. *Meth. Cell Biol.* **42**, 331-358.

Ludwig, T., Griffiths, G. and Hoflack, B. (1991). Distribution of newly synthesized lysosomal enzymes in the endocytic pathway of normal rat kidney cells. *J. Cell Biol.* **115**, 1561-1572.

Marchuk, D., Drumm, M., Saulino, A. and Collins, F. S. (1991). Construction of T-vectors, a rapid and general system for direct cloning of unmodified PCR products. *Nucl. Acids Res.* **19**, 1154.

Mellman, I. (1996). Endocytosis and molecular sorting. *Annu. Rev. Cell Dev. Biol.* **12**, 575-625.

Meresse, S., Gorvel, J. P. and Chavrier, P. (1995). The rab7 GTPase resides on a vesicular compartment connected to lysosomes. *J. Cell Sci.* **108**, 3349-3358.

Merion, M. and Sly, W. S. (1983). The role of intermediate vesicles in the adsorptive endocytosis and transport of ligand to lysosomes by human fibroblasts. *J. Cell Biol.* **96**, 644-650.

Morgenstern, J. P. and Land, H. (1990). Advanced mammalian gene transfer: high titre retroviral vectors with multiple drug selection markers and a complementary helper-free packaging cell line. *Nucl. Acids Res.* **18**, 3587-3596.

Mrini, A., Moukhles, H., Jacomy, H., Bosler, O. and Doucet, G. (1995). Efficient immunodetection of various protein antigens in glutaraldehyde-fixed brain tissue. *J. Histochem. Cytochem.* **43**, 1285-1291.

Mukherjee, S., Ghosh, R. N. and Maxfield, F. R. (1997). Endocytosis. *Physiol. Rev.* **77**, 759-803.

Mullock, B. M., Bright, N. A., Fearon, C. W., Gray, S. R. and Luzio, J. P. (1998). Fusion of lysosomes with late endosomes produces a hybrid organelle of intermediate density and is NSF dependent. *J. Cell Biol.* **140**, 591-601.

Odorizzi, G., Babst, M. and Emr, S. D. (1998). Fab1p PtdIns(3)P 5-kinase function essential for protein sorting in the multivesicular body. *Cell* **95**, 847-858.

Ohashi, M., de Vries, K. J., Frank, R., Snoek, G., Bankaitis, V., Wirtz, K. and Huttner, W. B. (1995). A role for phophatidylinositol transfer protein in secretory vesicle formation. *Nature* **377**, 544-547.

Ohashi, M., Miwako, I., Nakamura, K., Yamamoto, A., Murata, M., Ohnishi, S. and Nagayama, K. (1999). An arrested late endosome-lysosome intermediate aggregate observed in a Chinese hamster ovary cell mutant isolated by novel three-step screening. *J. Cell Sci.* **112**, 1125-1138.

Ohashi, M., Murata, M. and Ohnishi, S. (1992). A novel fluorescence method to monitor the lysosomal disintegration of low density lipoprotein. *Eur. J. Cell Biol.* **59**, 116-126.

Pagano, R. E., Martin, O. C., Kang, H. C. and Haugland, R. P. (1991). A novel fluorescent ceramide analogue for studying membrane traffic in animal cells: accumulation at the Golgi apparatus results in altered spectral properties of the sphingolipid precursor. *J. Cell Biol.* **113**, 1267-1279.

Parton, R. G., Simons, K. and Dotti, C. G. (1992). Axonal and dendritic endocytic pathways in cultured neurons. *J. Cell Biol.* **119**, 123-137.

Phillips, S. E., Sha, B., Topalof, L., Xie, Z., Alb, J. G., Klenchin, V. A., Swigart, P., Cockcroft, S., Martin, T. F., Luo, M. et al. (1999). Yeast Sec14p deficient in phosphatidylinositol transfer activity is functional in vivo. *Mol. Cell* **4**, 187-197.

Press, B., Feng, Y., Hoflack, B. and Wandinger-Ness, A. (1998). Mutant rab7 causes the accumulation of cathepsin D and cation-independent mannose 6-phosphate receptor in an early endocytic compartment. *J. Cell Biol.* **140**, 1075-1089.

Pryer, N. K., Wuestehube, L. J. and Schekman, R. (1992). Vesicle-mediated protein sorting. *Annu. Rev. Biochem.* **61**, 471-516.

Puri, V., Watanabe, R., Dominguez, M., Sun, X., Wheatley, C. L., Marks, D. L. and Pagano, R. E. (1999). Cholesterol modulates membrane traffic along the endocytic pathway in sphingolipid-storage diseases. *Nature Cell Biol.* **1**, 386-388.

Robinson, L. J., Aniento, F. and Gruenberg, J. (1997). NSF is required for transport from early to late endosomes. *J. Cell Sci.* **110**, 2079-2087.

Schekman, R. (1992). Genetic and biochemical analysis of vesicular traffic in yeast. *Curr. Opin. Cell Biol.* **4**, 587-592.

Schimmoller, F. and Riezman, H. (1993). Involvement of Ypt7p, a small GTPase, in traffic from late endosome to the vacuole in yeast. *J. Cell Sci.* **106**, 823-830.

Storrie, B. and Desjardins, M. (1996). The biogenesis of lysosomes: is it a kiss and run, continuous fusion and fission process? *BioEssays* **18**, 895-903.

Thery, C., Regnault, A., Garin, J., Wolfers, J., Zitvogel, L., Ricciardi-Castagnoli, P., Raposo, G. and Amigorena, S. (1999). Molecular Characterization of dendritic cell-derived exosomes: selective accumulation of the heat shock protein hsc73. *J. Cell Biol.* **147**, 599-610.

Ueno, T., Ishidoh, K., Mineki, R., Tanida, I., Murayama, K., Kadowaki, M. and Kominami, E. (1999). Autolysosomal membrane-associated betaine homocysteine methyltransferase. Limited degradation fragment of a sequestered cytosolic enzyme monitoring autophagy. *J. Biol. Chem.* **274**, 15222-15229.

Vitelli, R., Chiariello, M., Lattero, D., Bruni, C. B. and Bucci, C. (1996). Molecular cloning and expression analysis of the human Rab7 GTP-ase complementary deoxyribonucleic acid. *Biochem. Biophys. Res. Commun.* **229**, 887-890.

Vitelli, R., Santillo, M., Lattero, D., Chiariello, M., Bifulco, M., Bruni, C. B. and Bucci, C. (1997). Role of the small GTPase Rab7 in the late endocytic pathway. *J. Biol. Chem.* **272**, 4391-4397.

Yamashiro, D. J., Tycko, B., Fluss, S. R. and Maxfield, F. R. (1984). Segregation of transferrin to a mildly acidic (pH 6. 5) para-Golgi compartment in the recycling pathway. *Cell* **37**, 789-800.